

Liu, Shang, Ronghui Zhang, Dezong Zhao, and Houbing Song. "Adaptive Dual-Channel Event-Triggered Fuzzy Control for Autonomous Underwater Vehicles With Multiple Obstacles Environment." IEEE Transactions on Intelligent Transportation Systems, 2024, 1–14.
<https://doi.org/10.1109/TITS.2024.3387999>.

<https://doi.org/10.1109/TITS.2024.3387999>

© 2024 IEEE. Personal use of this material is permitted. Permission from IEEE must be obtained for all other uses, in any current or future media, including reprinting/republishing this material for advertising or promotional purposes, creating new collective works, for resale or redistribution to servers or lists, or reuse of any copyrighted component of this work in other works.

Access to this work was provided by the University of Maryland, Baltimore County (UMBC) ScholarWorks@UMBC digital repository on the Maryland Shared Open Access (MD-SOAR) platform.

Please provide feedback

Please support the ScholarWorks@UMBC repository by emailing scholarworks-group@umbc.edu and telling us what having access to this work means to you and why it's important to you. Thank you.

Adaptive Dual-Channel Event-Triggered Fuzzy Control for Autonomous Underwater Vehicles With Multiple Obstacles Environment

Shang Liu^{1b}, Ronghui Zhang^{1b}, Dezong Zhao^{1b}, *Senior Member, IEEE*, and Houbing Song^{1b}, *Fellow, IEEE*

Abstract—This article investigates the formation control of autonomous underwater vehicles (AUVs) suffering from unknown sea loads, unmoulded structure, limited communication and multiple static and moving obstacles. Given the challenge, a novel adaptive dual-channel event-triggered control scheme is proposed for formation tracking and obstacles avoidance. To economize the communication resources, the dual-channel event-triggered mechanism is designed in the sensor-to-controller and controller-to-actuator channels respectively. By adopting the approximation of fuzzy systems in the form of one-parameter integrated learning, the uncertainties consisted of the unmoulded structure and unknown sea loads are compressed together to be compensated online, which ensures a lower computational cost. To solve the multiple obstacles, the modified artificial potential field approach is employed, and the derived repulsive potential field can ensure that the multi-AUV formation can avoid obstacles smoothly regardless of static or moving obstacles. It is showed by the Lyapunov stability theorem that the tracking errors are guaranteed to be semi-globally uniformly ultimately bounded. Finally, three simulation examples illustrate the effectiveness and superiority of the proposed scheme.

Index Terms—Autonomous underwater vehicle, event-triggered control, adaptive fuzzy control, obstacle avoidance.

I. INTRODUCTION

THE utilization of deep-sea resources has led to an escalating demand for autonomous underwater vehicles (AUVs), which are now playing an increasingly pivotal role in commercial, scientific, and other various fields [1], [2]. Compared to

the path tracking of a single AUV, steering a collaborative group of AUVs offers significant advantages for executing complex underwater tasks. The research on multiple AUVs has attracted increasing attention from the marine control field in recent decades [3], [4], [5]. Note that, the existing research on the cluster of AUVs is mainly concentrated on how to maintain the specified formation while tracking the given reference trajectory. Plenty of useful control strategies are developed for the formation tracking problem, which can be generally divided into four categories, including behavior-based [6], virtual structure [7], leader-following [8] and graph-based [9].

However, several fundamental challenges related to the multi-AUV formation have not been fully resolved, including navigating around obstacles, economizing limited communication resources, handling with uncertainties caused by sea loads and unknown structures, and so on. In the complex deep-sea environment, the multi-AUV formation will inevitably encounter various statics (such as rocks and shipwrecks) and moving obstacles (such as fish) when performing underwater tasks, which may threaten the safety of the formation. Currently, there are several collision avoidance methods in open literature on multi-AUV systems, such as the artificial potential field (APF) [10], deep reinforcement learning (DRL) [11], robust predictive control [12], rapidly exploring random trees (RRTs) [13] etc. It is worth noting that most of the planning techniques mentioned above are rooted in offline optimization schemes, primarily designed for static or quasi-static operating environments. Their output is typically a set of waypoints or trajectories that are optimal in terms of energy consumption while meeting certain environmental constraints [14]. However, in a real-time environment with multiple obstacles, AUVs operate within a partially known dynamic environment. This means that the knowledge of the operating workspace is continually updated online through onboard multibeam sensors. In such circumstances, the AUVs must be able to dynamically recalculate their reference paths in response to possible environmental changes.

As for the controller design, the formation control of AUVs is a highly nonlinear problem, where the uncertainties including unknown sea loads and unmoulded structure are imposed. Since ocean currents are unpredictable, the hydrodynamic damping coefficients and sea loads become unknown and time-varying, which increases the complexity of the controller design [15]. To mitigate the uncertainties of AUVs, multiple approaches are widely adopted, including

Manuscript received 25 October 2023; revised 1 March 2024; accepted 9 April 2024. This work was supported in part by the National Natural Science Foundation of China under Grant 52172350 and Grant 51775565, in part by Guangdong Basic and Applied Research Foundation under Grant 2021B1515120032 and Grant 2022B1515120072, in part by Guangzhou Science and Technology Plan Project under Grant 2024B01W0079, in part by Nansha Key Research and Development Program under Grant 2022ZD014, and in part by the Science and Technology Planning Project of Guangdong Province under Grant 2023B1212060029. The Associate Editor for this article was Z. Li. (Corresponding author: Ronghui Zhang.)

Shang Liu is with Guangdong Key Laboratory of Intelligent Transportation System, School of Intelligent Systems Engineering, Sun Yat-sen University, Guangdong 510275, China, and also with the College of Information Science and Engineering, Northeastern University, Shenyang, Liaoning 110000, China (e-mail: dliushang@gmail.com).

Ronghui Zhang is with Guangdong Key Laboratory of Intelligent Transportation System, School of Intelligent Systems Engineering, Sun Yat-sen University, Guangdong 510275, China (e-mail: zhangrh25@mail.sysu.edu.cn).

Dezong Zhao is with the James Watt School of Engineering, University of Glasgow, G12 8QQ Glasgow, U.K. (e-mail: dezong.zhao@glasgow.ac.uk).

Houbing Song is with the Department of Information Systems, University of Maryland, Baltimore County (UMBC), Baltimore, MD 21250 USA (e-mail: h.song@ieee.org).

Digital Object Identifier 10.1109/TITS.2024.3387999

1558-0016 © 2024 IEEE. Personal use is permitted, but republication/redistribution requires IEEE permission.

See <https://www.ieee.org/publications/rights/index.html> for more information.

adaptive estimation [16], neural network (NN) [17], [18] or fuzzy system (FS) approximation [19], sliding mode control [20], nonlinear model predictive control (NMPC) [21], [22], [23]. Although the system uncertainty can be effectively approximated by using the NN/FS with an adaptive method, it is noted that the *priori* knowledge of the inertial mass of AUVs is still required, as outlined in [17], [18], and [19]. Besides, the aforementioned approximation approaches employ the approximating capability of NN and FS. Unfortunately, this inevitably weakens the robustness against the influence of sea loads. In addition, as the number of hidden layer nodes increases, the existing adaptive fuzzy control method necessitates continual updates to the online learning weights, thereby increasing the computational load.

Undoubtedly, the AUVs are suffered from the excessive wear of actuators and communication channel clogging during long-term operations in the harsh deep ocean environment. Event-triggered control (ETC) provides a promising technique to obtain the satisfactory control performance with the limited communication bandwidth, which leads to an extensive attention in various control communities [24], [25], [26], [27], [28]. For example, a fixed threshold event-triggered (FTETC) mechanism was designed in [24] to reduce communication frequency from the controller to actuators, thereby alleviating wear on the actuators. Aiming at the nonlinear strict-feedback system, [25] developed an output feedback control strategy by incorporating of the FTETC and NN-based state observer. To apply the ETC approach to the marine vehicles, [26] developed a network-based weighted event-triggered control strategy for the dynamic positioning of unmanned surface vehicles. As for the AUV system, some fruitful works can be found in [29], [30], [31], and [32]. To name a few, [29] designed an event-triggered security control protocol for the multi-AUV formation by using the FTETC, where the denial-of-service attack was effectively solved. Furthermore, a sectionalized event-triggered mechanism (SETM) was developed in [30], which could enhance the robustness of the transient phase. However, the aforementioned ETC schemes mainly focus on releasing the communication resources of the controller-to-actuator (C-A) channel, but cannot guarantee the saving of the communication resources of the sensor to the controller (S-C) channel. This means that the channel bandwidth cannot be sufficiently economized to save communication resources.

In this sense, the formation control of AUVs continues to pose a significant challenge to the field of marine control, especially when considering the high-demand tasks envisaged by the marine industry. Based on above discussion, some core challenges are concluded as follow: i)

- 1) During the underwater missions, the AUV inevitably suffers from the obstacles avoidance. Although there exist some useful obstacle-free methods [10], [11], [12], [13], the majority of these methods are based on the off-line optimization scheme and only consider static or quasi-static obstacle environments.
- 2) The tracking performance of the multi-AUV formation is affected by some unfavorable factors such as system uncertainty and sea loads. Despite the use of the NN or

FS approximating methods in [17], [18], and [19], the continuous updates to online learning weights are necessary, resulting in a significant computational burden.

- 3) The frequent execution of control signals by the propulsion system of AUVs may cause the excessive mechanical wear of actuators and the clogging of communication channels, especially during long-term underwater operations. The emerging ETC for AUVs is an effective tool [29], [30], [31], [32], but to date, there is no effective ETC method capable of simultaneously triggering both the C-A and S-C channels.

Inspired by the above observation, this paper focuses on the AUV formation control problem suffering from the limited communication constraint, multiple obstacles avoidance, unknown system uncertainty and sea loads. Consequently, an adaptive dual-channel event-triggered fuzzy control scheme is proposed. The main contributions are summarized as threefold:

- i) A modified artificial potential field (MAPF) approach is proposed to realize the collision-free formation tracking for AUVs in a real-time way, despite of the influence of static and moving obstacles.
- ii) Without the *priori* knowledge of AUV model, a one-parameter integrated learning method is introduced to simplify the weight updating process of adaptive fuzzy control. This simplification applies when approximating uncertainties that include unknown sea loads and unmodeled structures, resulting in a significant reduction in computational burden.
- iii) Unlike previous ETC studies [29], [30], [31], [32], a novel dual-channel event-triggered mechanism (DCETM) is proposed for AUVs. The designed DCETM simultaneously triggers both the C-A and S-C channels, effectively reducing the transmission frequency of control signals in both channels and alleviating the mechanical wear on actuators.

Notation: Throughout this paper, $|\cdot|$ denotes the absolute operator value of a scalar (\cdot). $\|\cdot\|$ denotes the Euclidean norm of a vector. $\tilde{(\cdot)} = \hat{(\cdot)} - (\cdot)$, where $\hat{(\cdot)}$ denotes the estimation value of (\cdot).

II. PROBLEM FORMULATION

A. AUV Modeling

In this paper, the three degrees of freedom (3)-DOFs vertical motion of AUV is considered, assuming reasonably that the rolling angle ϕ and yawing angle ψ are relatively small [1]. Neglecting the motion elements of sway, roll and yaw, a team of AUVs described in two frameworks, i.e., the earth-fixed and body-fixed frameworks, are considered. Considering a group of AUVs $i = 1, 2, \dots, N$, the kinematic equation of i -th underactuated AUV can be established as (1), and the illustrative variables is exhibited in Fig. 1.

$$\dot{\eta}_i = \mathbf{R}(\eta_i) \mathbf{v}_i \quad (1)$$

where $\eta_i = [x_i, z_i, \theta_i]^T$ denotes the X-Z coordinate surge, heave displacement and pitch angle in the earth-fixed framework, and $\mathbf{v}_i = [u_i, w_i, q_i]^T$ represents the vector of surge

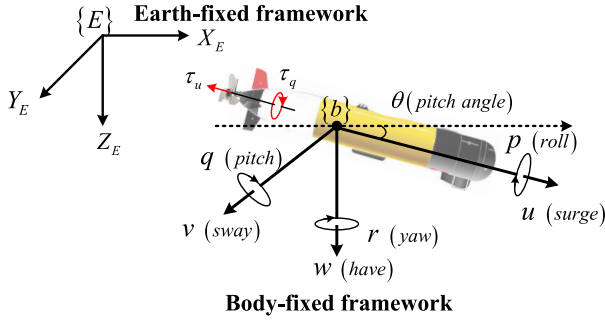


Fig. 1. The motion coordinate system for the AUV.

speed, heave speed and pitch rate in the body-fixed framework, respectively. $R(\eta_i)$ denotes the rotation matrix in pitch motion which can be expressed as

$$R(\eta_i) = \begin{bmatrix} \cos \theta_i & -\sin \theta_i & 0 \\ \sin \theta_i & \cos \theta_i & 0 \\ 0 & 0 & 1 \end{bmatrix}$$

The dynamic model of the 3-DOFs AUV can be expressed as (2).

$$M_i \dot{v}_i + C_i(v_i)v_i + D_i(v_i)v_i + g_i = \tau_{si} + \tau_i \quad (2)$$

where M_i denotes the inertia matrix, $D_i(v_i)$ is the hydrodynamic damping matrix, $C_i(v_i)$ denotes the Coriolis-centripetal matrix including add mass, which can be expressed as follows.

$$M_i = \begin{bmatrix} m_{11} & 0 & 0 \\ 0 & m_{22} & 0 \\ 0 & 0 & m_{33} \end{bmatrix}, D_i(v_i) = \begin{bmatrix} d_{11} & 0 & 0 \\ 0 & d_{22} & 0 \\ 0 & 0 & d_{33} \end{bmatrix}$$

$$C_i(v_i) = \begin{bmatrix} 0 & 0 & -m_{22}w_i \\ 0 & 0 & m_{11}u_i \\ m_{22}w_i & -m_{11}u_i & 0 \end{bmatrix}$$

The gravitational and buoyancy forces are assumed to out-balance each other such that the restoring force such that $g_i = 0$. $\tau_i = [\tau_{ui}, 0, \tau_{qi}]^T \in \mathbb{R}^3$ denotes the system input, where τ_{ui} denotes the thrust and τ_{qi} is the turning torque. $\tau_{si} = [\tau_{s1i}, \tau_{s2i}, \tau_{s3i}]^T \in \mathbb{R}^3$ represents the unknown sea loads induced by ocean currents. Due to the uncertainty of M_i , $D_i(v_i)$, $C_i(v_i)$, the unmolded structure can be constructed as $[f_{ui}(v), f_{wi}(v), f_{qi}(v)]^T = M_i^{-1}(-C_i(v_i)v_i - D_i(v_i)v_i)$. Then, the kinematical and dynamic model can be rewritten as (3) and (4).

$$\begin{cases} \dot{x}_i = u_i \cos \theta_i - w_i \sin \theta_i \\ \dot{z}_i = u_i \sin \theta_i + w_i \cos \theta_i \\ \dot{\theta}_i = q_i \end{cases} \quad (3)$$

$$\begin{cases} \dot{u}_i = -f_{ui}(v) + \frac{1}{m_{ui}}\tau_{ui} + \frac{1}{m_{ui}}\tau_{sui} \\ \dot{w}_i = -f_{wi}(v) + \frac{1}{m_{wi}}\tau_{swi} \\ \dot{q}_i = -f_{qi}(v) + \frac{1}{m_{qi}}\tau_{qi} + \frac{1}{m_{qi}}\tau_{sqi} \end{cases} \quad (4)$$

Some useful assumptions and lemma are given as follows.

Control Objective: The AUVs are tasked with achieving formation tracking in a multi-obstacle environment and attaining

a desired formation configuration defined by relative positions and orientations as follows:

$$\lim_{t \rightarrow \infty} \|\eta_i(t) - \Delta_i - \eta_d(t)\| \leq \varepsilon_0$$

where $\varepsilon_0 \in \mathbb{R}$ is a small positive constant. The coordinate transformation $\Delta_i = [\Delta x_i, \Delta z_i, \Delta q_i]^T \in \mathbb{R}^3$ can be expressed as $\Delta_i = [\rho_{di} \cos \lambda_{di}, \rho_{di} \sin \lambda_{di}, 0]^T \in \mathbb{R}^3$, representing the vector that defines the configuration of each AUV in the formation. Here, ρ_{di} represents the desired range, and λ_{di} denotes the desired bearing angle. $\eta_d = [x_d, z_d, \theta_d]^T \in \mathbb{R}^3$ denotes the desired reference path generated by the virtual underwater vehicle, which will be defined in Section III.

Assumption 1 ([15]): The vector of unknown sea loads τ_{si} satisfies $\|\tau_{si}\| \leq \tau_{sM}$, where τ_{sM} denotes an unknown positive constant.

Assumption 2 ([8]): The reference path $\eta_d(t)$ and its derivative $\dot{\eta}_d(t)$ are smooth and bounded functions, i.e., there exist positive constants Y_1 and Y_2 such that $\|\eta_d(t)\| \geq Y_1$, $\|\dot{\eta}_d(t)\| \geq Y_2$, $\forall t > 0$.

Assumption 3 ([2]): It is assumed that the AUV can detect the status information of obstacles within a measurable range, including coordinate position, relative distance and bearing angle. In marine practice, the relevant data can be obtained through the onboard sensing devices, such as inertial navigation systems (INS), light detection and ranging (LIDAR), sonar sensors, and others.

Lemma 1 ([33]): Consider a nonlinear system described as $\dot{x}(t) = F(x(t))$. Let the function $V(t) > 0$, $\forall t \in \mathbb{R}^+$ be a continuous function, and $V(0)$ is bounded. If the inequality $\dot{V}(t) \leq -\kappa_0 V(t) + \varrho_0$ holds, with κ_0 and ϱ_0 being positive constants, then the following inequality can be deduced.

$$V(t) \leq V(0)e^{-\kappa_0 t} + \frac{\varrho_0}{\kappa_0} (1 - e^{-\kappa_0 t})$$

The solution of the nonlinear system is said to be semi-globally uniform ultimate bounded (SGUUB), if for any initial state $x_0 = x(t_0) \in \Omega \subset \mathbb{R}^n$, the above inequality is satisfied and there exists a constant a_0 and a time constant $T = T(a_0, x_0)$, for all $t \in [t_0 + T, +\infty)$, $\|x\| \leq a_0$.

B. Fuzzy System Approximation

A FS consists of a fuzzy rule base, a fuzzifier, and a defuzzifier. Let F_i^l be the fuzzy sets for a state χ_i , and define its membership functions as $\mu_{F_i^l}^l$ with $i = 1, \dots, N$. The fuzzy rule base consists of the If-Then inference rule [34], that is, R^l : If χ_1 is F_1^l and χ_2 is F_2^l and \dots and χ_N is F_N^l , then y is G^l , $l = 1, 2, \dots, n$. Then, one can calculate the FS as

$$y(\chi) = \frac{\sum_{l=1}^n \bar{y}_l \prod_{i=1}^N \mu_{F_i^l}^l(\chi_i)}{\sum_{l=1}^n [\prod_{i=1}^N \mu_{F_i^l}^l(\chi_i)]}$$

where $\bar{y}_l = \max_{y \in R} \mu_{G^l}(y)$ with $\mu_{G^l}(y)$ being the membership functions, and $\chi = [\chi_1, \dots, \chi_N]^T$. By defining $\Theta^T = [\Theta_1, \dots, \Theta_n] = [\bar{y}_1, \dots, \bar{y}_n]$ and $S(\chi) = [s_1(\chi), \dots, s_n(\chi)]^T$ where $s_l(\chi)$ is given by $s_l(\chi) = \frac{\prod_{i=1}^N \mu_{F_i^l}^l(\chi_i)}{\sum_{l=1}^n [\prod_{i=1}^N \mu_{F_i^l}^l(\chi_i)]}$ and ensuring that $\|S(\chi)\| \leq S^*$, with S^* being a positive constant, the FS set can be calculated as $y(\chi) = \Theta^T S(\chi)$. In this work, the FS approximation can be

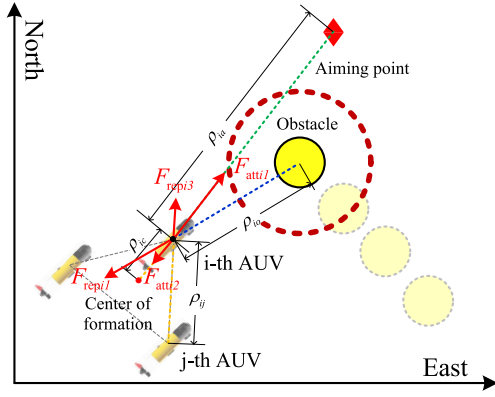


Fig. 2. The framework of the proposed MAPF algorithm.

introduced as Lemma 2, which will be useful in the control design.

Lemma 2 ([34]): For any given continuous function $f(\chi)$ with $f(\mathbf{0}) = 0$ defined on a compact set Ω_F , the nonlinear function $f(\chi)$ can be remodeled as (5) with random approximation error $\varepsilon > 0$.

$$\sup_{\chi \in \Omega_F} |f(\chi) - \Theta^T S(\chi)| \leq \varepsilon \quad (5)$$

III. PATH PLANNING OF MODIFIED ARTIFICIAL POTENTIAL FUNCTION ALGORITHM

To enhance the safety of deep-sea operations, a MAPF planning method is proposed for the multi-AUV formation, which takes into account the avoidance of static obstacle, the avoidance of moving obstacle and the collision between AUVs. In marine practice, AUVs inevitably encounter various obstacles and intra-formation collisions. Using the artificial potential function to calculate the attractive or repulsive force of AUVs is a simple and effective method, which can be used for the formation tracking control [35]. In the algorithm, each AUV is treated as an isolated particle within a potential well. All obstacles are considered objects exerting repulsive forces on AUVs, while aiming points are regarded as objects with attractive forces. The potential function is a nonnegative function $U_i(x, z)$ which is consisted by two kinds of force fields, i.e., the attractive field $U_{atti}(x, z)$ generated by the aiming point and the repulsive force field $U_{repi}(x, z)$ generated by the encountering obstacles and adjacent AUVs, which can be expressed as $U_i(x, z) = U_{atti}(x, z) + U_{repi}(x, z)$. The schematic diagram of the proposed MAPF algorithm is presented in Fig.2.

Different from the traditional artificial potential function for a single AUV, the attractive field $U_{atti}(x, z)$ designed for multi-AUV formation can be calculated as (6). It is noted that $U_{atti}(x, z)$ consists of two parts, i.e., U_{atti1} and U_{atti2} . U_{atti1} is responsible for generating an attractive force that guides the AUVs towards the desired position. To avoid formation splitting, the attractive potential function U_{atti2} is introduced between the flockmates when the AUV deviate from the center of formation configuration, i.e., $\rho_{ic} > \rho_{di}$. ρ_{ic} denotes the distance between the i -th AUV and the center

of formation.

$$U_{atti}(x, z) = \begin{cases} U_{atti1}(x, z) + U_{atti2}(x, z), & \rho_{ic} > \rho_{di} \\ U_{atti1}(x, z), & \rho_{ic} \leq \rho_{di} \end{cases} \quad (6)$$

with

$$U_{atti1}(x, z) = \frac{1}{2} k_{att1} \rho_{ia}^2, \quad U_{atti2}(x, z) = \frac{1}{2} k_{att2} \rho_{ic}^2$$

where ρ_{ia} denotes the relative distance between the i -th AUV and the position of aiming point. ρ_{ic} denotes the relative distance between the i -th AUV and the position of the formation's geometric center. k_{att1} and k_{att2} are positive scaling factors set by user.

Subsequently, the attractive force can be derived as the negative gradient of the attractive potential function, which can be formulated as can be expressed as

$$F_{atti}(x, z) = \begin{cases} F_{atti1}(x, z) + F_{atti2}(x, z), & \rho_{ic} > \rho_{di} \\ F_{atti1}(x, z), & \rho_{ic} \leq \rho_{di} \end{cases} \quad (7)$$

with

$$F_{atti1}(x, z) = -\nabla U_{atti1} = k_{att1} \rho_{ia} \mathbf{n}_{ia}$$

$$F_{atti2}(x, z) = -\nabla U_{atti2} = k_{att2} \rho_{ic} \mathbf{n}_{ic}$$

where \mathbf{n}_{ia} and \mathbf{n}_{ic} are two unit vectors pointing from the i -th AUV to the aiming point and from the i -th AUV to the geometric center of the formation configuration, respectively.

Similarly, to avoid the external obstacles and collision among the AUVs, the repulsive force field $U_{repi}(x, z)$ can be constructed as (8) with piecewise function form. To be specific, the repulsive potential function $U_{repi}(x, z)$ consists of two parts, i.e., U_{repi1} is used to avoid the external obstacles while $U_{repi2,j}$, $j \in \mathcal{N}_i^c$ is designed to avoid the collision among AUVs, with \mathcal{N}_i^c being the aggregation of the i -th AUV at risk of collision within the formation.

$$U_{repi} = \begin{cases} U_{repi1} + \sum_{j \in \mathcal{N}_i^c} U_{repi2,j}, & \rho_{io} \leq d_o, \rho_{ij} \leq 2R \\ U_{repi1}, & \rho_{io} \leq d_o, \rho_{ij} > 2R \\ \sum_{j \in \mathcal{N}_i^c} U_{repi2,j}, & \rho_{io} > d_o, \rho_{ij} \leq 2R \\ 0, & \rho_{io} > d_o, \rho_{ij} > 2R \end{cases} \quad (8)$$

with

$$U_{repi1} = \frac{1}{2} k_{rep1} \left(\frac{1}{\rho_{io}} - \frac{1}{d_o} \right) \rho_{ia}^2$$

$$U_{repi2,j} = \frac{1}{2} k_{rep2} \left(\frac{1}{\rho_{ij}} - \frac{1}{2R} \right) \rho_{ic}^2$$

where ρ_{io} denotes the relative distance between the i -th AUV and obstacles. d_o represents the safety distance between obstacles and the AUV. ρ_{ij} indicates the distance between the i -th AUV and the neighboring j -th AUV. R denotes the safety radius for each AUV. k_{rep1} and k_{rep2} are positive repulsive force factors.

Then, by calculating the negative gradient of the repulsive potential function, the repulsive force F_{repi} can be derived as

$$F_{\text{repi}} = -\nabla U_{\text{repi}} = \begin{cases} F_{\text{repi}1} + F_{\text{repi}2} + \sum_{j \in \mathcal{N}_i^c} \{F_{\text{repi}3,j} + F_{\text{repi}4,j}\}, & \rho_{io} \leq d_o, \rho_{ij} \leq 2R \\ F_{\text{repi}1} + F_{\text{repi}2}, & \rho_{io} \leq d_o, \rho_{ij} > 2R \\ \sum_{j \in \mathcal{N}_i^c} \{F_{\text{repi}3,j} + F_{\text{repi}4,j}\}, & \rho_{io} > d_o, \rho_{ij} \leq 2R \\ 0, & \rho_{io} > d_o, \rho_{ij} > 2R \end{cases} \quad (9)$$

with

$$\begin{cases} F_{\text{repi}1} = k_{\text{rep}1} \left(\frac{1}{d_o} - \frac{1}{\rho_{io}} \right) \frac{1}{\rho_{io}^2} \rho_{ia}^2 \mathbf{n}_{oi} \\ F_{\text{repi}2} = \frac{k_{\text{rep}1}}{2} \left(\frac{1}{\rho_{io}} - \frac{1}{d_o} \right) \rho_{ia} \mathbf{n}_{ia} \\ F_{\text{repi}3,j} = k_{\text{rep}2} \left(\frac{1}{2R} - \frac{1}{\rho_{ij}} \right) \frac{1}{\rho_{ij}^2} \rho_{ic}^2 \mathbf{n}_{ji} \\ F_{\text{repi}4,j} = \frac{k_{\text{rep}2}}{2} \left(\frac{1}{\rho_{ij}} - \frac{1}{2R} \right) \rho_{ic} \mathbf{n}_{ic} \end{cases}$$

where $F_{\text{repi}1}$ denotes the repulsive force to prevent collisions of external obstacles, $F_{\text{repi}3}$ is the repulsive force to prevent collisions between AUVs, $F_{\text{repi}2}$ and $F_{\text{repi}4}$ are derived from the repulsion function to avoid the AUV falling into a local minimum [36]. \mathbf{n}_{oi} and \mathbf{n}_{ji} are two unit vectors pointing from obstacles to the i -th AUV and from the neighboring j -th AUV to the i -th AUV. As a result, the final resultant force is calculated as $F_i(x, z) = F_{\text{atti}}(x, z) + F_{\text{repi}}(x, z)$. Define the angle of resultant force θ_F as the desired pitch angle of AUV, and the dynamics of the reference path can be calculated as

$$\begin{cases} \dot{x}_d = u_d \cos \theta_F - w_d \sin \theta_F \\ \dot{z}_d = u_d \sin \theta_F + w_d \cos \theta_F \end{cases} \quad (10)$$

The corresponding desired azimuth angle of AUV can be expressed as

$$\theta_d = 0.5 \text{sgn}(z_d - z_i) \pi [1 - \text{sgn}(x_d - x_i)] + \arctan\left(\frac{z_d - z_i}{x_d - x_i}\right) \quad (11)$$

Hence, based on (10) and (11), the kinematic tracking errors can be defined as

$$\begin{aligned} x_{ei} &= x_d + \Delta x_i - x_i, & z_{ei} &= z_d + \Delta z_i - z_i \\ \theta_{ei} &= \theta_d + \Delta \theta_i - \theta_i, & \chi_{ei} &= \sqrt{x_{ei}^2 + z_{ei}^2} \end{aligned} \quad (12)$$

Finally, the kinematic tracking errors x_{ei} , z_{ei} and θ_{ei} will be used to design the controller in the next section.

IV. THE ADAPTIVE DUAL-CHANNEL EVENT-TRIGGERED FUZZY CONTROL SCHEME

In this section, an adaptive dual-channel event-triggered fuzzy formation control scheme is proposed for AUVs.

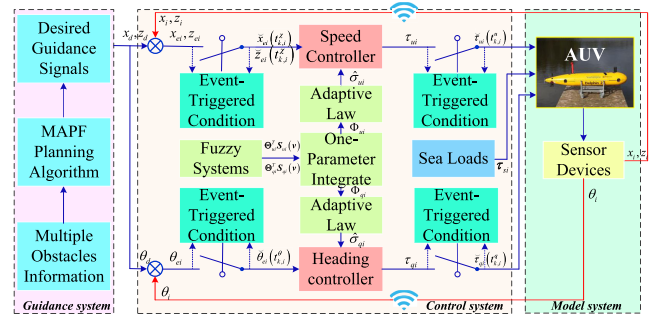


Fig. 3. The conceptual signal flow diagram of the proposed scheme.

Using the reference path signals in III, the control design is exhibited in the following order: the DCETM is devised in Section IV-A, and the control design process is shown in Section IV-B. Finally, the stability analysis is provided in Section IV-C. To show the control process intuitively, Fig.3 the conceptual signal flow diagram of the proposed control scheme.

A. Dual-Channel Event-Triggered Mechanism

This section introduces a novel DCETM for AUVs to reduce the actuator execution frequency and communication load. In contrast to existing ETC approaches for AUVs or other marine systems [26], [27], [28], [29], [30], [31], [32], the proposed DCETM enables simultaneous triggering of both the S-C and C-A channels. This innovation significantly decreases the communication channel's occupancy frequency.

Inspired by the input-based triggering condition [24], the event-triggering conditions of DCETM are designed as follows.

Triggering Condition 1 (S-C channel): In the S-C channel, the triggering condition 1 consists of two separated parts, i.e., the condition for position errors x_{ei} , z_{ei} and the condition for orientation error θ_{ei} , which are designed as (13).

$$\begin{cases} t_{k+1,i}^x = \inf\{t > t_{k,i}^x \mid |e_{xi}| \geq \xi_x |x_{ei}(t)| \wedge |e_{zi}| \geq \xi_z |z_{ei}(t)|\} \\ t_{k+1,i}^\theta = \inf\{t > t_{k,i}^\theta \mid |e_{\theta i}| \geq \xi_\theta |\theta_{ei}(t)|\} \end{cases} \quad (13)$$

where e_{xi} , e_{zi} , and $e_{\theta i}$ denote the measurement errors, which are defined as $e_{xi} = \check{x}_{ei}(t) - x_{ei}(t)$, $e_{zi} = \check{z}_{ei}(t) - z_{ei}(t)$, and $e_{\theta i} = \check{\theta}_{ei}(t) - \theta_{ei}(t)$. Additionally, ξ_x and ξ_θ are user-defined triggering threshold parameters. That is, when the triggering condition 1 is violated, the time instant will be marked as $t_{k+1,i}^x$ or $t_{k+1,i}^\theta$. At that point, the kinematic errors will be transformed to $\check{x}_{ei}(t_{k,i}^x)$, $\check{z}_{ei}(t_{k,i}^x)$ and $\check{\theta}_{ei}(t_{k,i}^\theta)$ and transmitted to the controller. The detailed formula is given as

$$\begin{cases} x_{ei}(t) = \check{x}_{ei}(t_{k,i}^x), z_{ei}(t) = \check{z}_{ei}(t_{k,i}^x), \forall t \in [t_{k,i}^x, t_{k+1,i}^x) \\ \theta_{ei}(t) = \check{\theta}_{ei}(t_{k,i}^\theta), \forall t \in [t_{k,i}^\theta, t_{k+1,i}^\theta) \end{cases} \quad (14)$$

Triggering Condition 2 (C-A channel): To reduce the executive frequency of actuators, the triggering condition 2 is designed in the C-A channel. Similarly, the triggering condition 2 consists of two separated parts, i.e., the condition for

the thrust τ_{ui} and the condition for the turning torque τ_{qi} . The corresponding formula can be designed as

$$\begin{cases} t_{k+1,i}^u = \inf \{t > t_{k,i}^u \mid |e_{ui}(t)| \geq \xi_u |\tau_{ui}(t)|\} \\ t_{k+1,i}^q = \inf \{t > t_{k,i}^q \mid |e_{qi}(t)| \geq \xi_q |\tau_{qi}(t)|\} \end{cases} \quad (15)$$

where $e_{ui} = \check{\tau}_{ui}(t) - \tau_{ui}(t)$, $e_{qi} = \check{\tau}_{qi}(t) - \tau_{qi}(t)$ denote the measurement errors. ξ_u and ξ_q are triggering threshold parameters set by users. Note that, to reduce the updating frequency of control laws, the time instant will be marked as $t_{k+1,i}^u$ or $t_{k+1,i}^q$ and τ_{ui} , τ_{qi} will be transformed into $\check{\tau}_{ui}(t_{k,i}^u)$, $\check{\tau}_{qi}(t_{k,i}^q)$ only when the triggering condition 2 is violated. The detailed formula can be derived as

$$\begin{cases} \tau_{ui}(t) = \check{\tau}_{ui}(t_{k,i}^u), \quad \forall t \in [t_{k,i}^u, t_{k+1,i}^u) \\ \tau_{qi}(t) = \check{\tau}_{qi}(t_{k,i}^q), \quad \forall t \in [t_{k,i}^q, t_{k+1,i}^q) \end{cases} \quad (16)$$

From the triggering conditions (13) and (15), we know that the following inequalities always hold: $|\check{x}_{ei}(t) - x_{ei}(t)| \leq \xi_x |x_{ei}(t)|$, $|\check{z}_{ei}(t) - z_{ei}(t)| \leq \xi_x |z_{ei}(t)|$, $|\check{\theta}_{ei}(t) - \theta_{ei}(t)| \leq \xi_\theta |\theta_{ei}(t)|$, $|\check{\tau}_{ui}(t) - \tau_{ui}(t)| \leq \xi_u |\tau_{ui}(t)|$, and $|\check{\tau}_{qi}(t) - \tau_{qi}(t)| \leq \xi_q |\tau_{qi}(t)|$. Thus, there exist positive parameters $\varsigma_{\chi i}(t)$, $\varsigma_{\theta i}(t)$, $\varsigma_{ui}(t)$ and $\varsigma_{qi}(t) \in [-1, 1]$ such that

$$\begin{cases} \check{x}_{ei}(t) = (1 + \varsigma_{\chi i} \xi_x) x_{ei}(t) \\ \check{z}_{ei}(t) = (1 + \varsigma_{\chi i} \xi_x) z_{ei}(t) \\ \check{\theta}_{ei}(t) = (1 + \varsigma_{\theta i} \xi_\theta) \theta_{ei}(t) \\ \check{\tau}_{ui}(t) = (1 + \varsigma_{ui} \xi_u) \tau_{ui}(t) \\ \check{\tau}_{qi}(t) = (1 + \varsigma_{qi} \xi_q) \tau_{qi}(t) \end{cases} \quad (17)$$

B. Formulation of Control Design

Step 1: By defining $\check{x}_{ei} = \sqrt{\check{x}_{ei}^2 + \check{z}_{ei}^2}$ and according to (3), (12) and (17), the derivative of the kinematic errors are derived as

$$\begin{aligned} \dot{\check{x}}_{ei} &= (1 + \varsigma_{\chi i} \xi_x) (\dot{x}_d \cos \theta_d + \dot{z}_d \sin \theta_d - u_i \cos \theta_{ei} - w_i \sin \theta_{ei}) \\ \dot{\check{\theta}}_{ei} &= (1 + \varsigma_{\theta i} \xi_\theta) (\dot{\theta}_d - q_i) \end{aligned} \quad (18)$$

Then, two virtual control laws α_{ui} and α_{ri} are designed to stabilize the kinematic errors.

$$\begin{aligned} \alpha_{ui} &= \frac{-k_{\chi i} \check{x}_{ei} + \dot{x}_d \cos \theta_d + \dot{z}_d \sin \theta_d - w_i \sin \theta_{ei}}{\cos \theta_{ei}} \\ \alpha_{qi} &= k_{\theta i} \dot{\check{\theta}}_{ei} + \dot{\theta}_d \end{aligned} \quad (19)$$

where $k_{\chi i}$ and $k_{\theta i}$ are positive control parameters set by user. To avoid the so-called ‘‘explosion of complexity’’, the dynamic surface control (DSC) filters β_{ui} , β_{qi} are used to seek the substitutes for the original virtual control laws, which can be expressed as

$$\begin{aligned} t_{ui} \dot{\beta}_{ui} + \beta_{ui} &= \alpha_{ui}, \quad \beta_{ui}(0) = \alpha_{ui}(0) \\ t_{qi} \dot{\beta}_{qi} + \beta_{qi} &= \alpha_{qi}, \quad \beta_{qi}(0) = \alpha_{qi}(0) \end{aligned} \quad (20)$$

where t_{ui} and t_{qi} are time constants of the filters. By defining the errors of dynamic surface as $\zeta_{ui} = \alpha_{ui} - \beta_{ui}$ and

$\zeta_{qi} = \alpha_{qi} - \beta_{qi}$, it renders $\dot{\beta}_{ui} = -\zeta_{ui}/t_{ui}$ and $\dot{\beta}_{qi} = -\zeta_{qi}/t_{qi}$. Then, the derivative of ζ_{ui} and ζ_{qi} can be calculated as

$$\begin{aligned} \dot{\zeta}_{ui} &= \dot{\alpha}_{ui} - \dot{\beta}_{ui} \\ &= -\frac{\zeta_{ui}}{t_{ui}} + \frac{\partial \alpha_{ui}}{\partial x_i} \dot{x}_i + \frac{\partial \alpha_{ui}}{\partial z_i} \dot{z}_i + \frac{\partial \alpha_{ui}}{\partial x_d} \dot{x}_d + \frac{\partial \alpha_{ui}}{\partial z_d} \dot{z}_d \\ &\quad + \frac{\partial \alpha_{ui}}{\partial \theta_i} \dot{\theta}_i + \frac{\partial \alpha_{ui}}{\partial \theta_d} \dot{\theta}_d + \frac{\partial \alpha_{ui}}{\partial w_i} \dot{w}_i \\ &= -\frac{\zeta_{ui}}{t_{ui}} + B_{ui}(\cdot) \\ \dot{\zeta}_{qi} &= -\frac{\zeta_{qi}}{t_{qi}} + B_{qi}(\cdot) \end{aligned} \quad (21)$$

where $B_{ui}(\cdot)$ and $B_{qi}(\cdot)$ are continues functions, and there exists the positive constants M_{ui} and M_{qi} such that $|B_{ui}(\cdot)| \leq M_{ui}$ and $|B_{qi}(\cdot)| \leq M_{qi}$.

Step 2: Define the kinetic errors as $u_{ei} = \beta_{ui} - u_i$, $q_{ei} = \beta_{qi} - q_i$. By combining (4), the derivative of kinetic errors u_{ei} and q_{ei} can be calculated as

$$\begin{aligned} \dot{u}_{ei} &= \dot{\beta}_{ui} + f_{ui}(\mathbf{v}) - \frac{1}{m_{ui}} \tau_{ui} - \frac{1}{m_{ui}} \tau_{sui} \\ \dot{q}_{ei} &= \dot{\beta}_{qi} + f_{qi}(\mathbf{v}) - \frac{1}{m_{qi}} \tau_{qi} - \frac{1}{m_{qi}} \tau_{sqi} \end{aligned} \quad (22)$$

According to Lemma 2, the unmoulded structure $f_{ui}(\mathbf{v})$ and $f_{qi}(\mathbf{v})$ can be approximated as $f_{ui}(\mathbf{v}) = \Theta_{ui}^T \mathbf{S}_{ui}(\mathbf{v}) + \varepsilon_{ui}$ and $f_{qi}(\mathbf{v}) = \Theta_{qi}^T \mathbf{S}_{qi}(\mathbf{v}) + \varepsilon_{qi}$ with random approximation errors ε_{ui} and ε_{qi} . To simplify the weight updating of adaptive fuzzy control, the one-parameter integrated learning method is introduced to approximate the unknown sea loads τ_{sui} , τ_{sqi} and unmoulded structures $f_{ui}(\mathbf{v})$, $f_{qi}(\mathbf{v})$ together. Using the Assumption 1, the corresponding unknown terms can be compressed as

$$\begin{aligned} f_{ui}(\mathbf{v}) - \frac{\tau_{sui}}{m_{ui}} &\leq \|\Theta_{ui}^T\| \|\mathbf{S}_{ui}(\mathbf{v})\| + \varepsilon_{uM} + \frac{\tau_{sum}}{m_{ui}} \\ &\leq \Xi_{ui} \phi_{ui}(\mathbf{v}) \\ f_{qi}(\mathbf{v}) - \frac{\tau_{sqi}}{m_{qi}} &\leq \Xi_{qi} \phi_{qi}(\mathbf{v}) \end{aligned} \quad (23)$$

with

$$\Xi_{ii} = \max \left\{ \|\Theta_{ii}\|, \frac{\tau_{sLM}}{m_{ii}} + \varepsilon_{LM} \right\}$$

$$\phi_{ii}(\mathbf{v}) = 1 + \|\mathbf{S}_{ii}(\mathbf{v})\|, \quad i = u, q$$

where ε_{LM} denotes the upper bounded variable of the approximation error. τ_{sLM} is the upper bound of unknown sea load. It is noted that, after dealing with the uncertainties by (23), both the unmolded structure and the sea loads can be divided into the product of two separate parts, i.e., Ξ_{ii} denotes the unknown terms required to be compensated by adaption and $\phi_{ii}(\mathbf{v})$ is the knowable term used for the control design.

Then, by using the Young's inequality, we have

$$\begin{aligned} |u_{ei}| \Xi_{ui} \phi_{ui}(\mathbf{v}) &\leq \frac{\Xi_{ui}^2 \phi_{ui}^2 u_{ei}^2}{4b_{ui}} + b_{ui} = \frac{\sigma_{ui} \Phi_{ui} u_{ei}^2}{(1 + \varsigma_{ui} \xi_u) m_{ui}} + b_{ui} \\ |q_{ei}| \Xi_{qi} \phi_{qi}(\mathbf{v}) &\leq \frac{\Xi_{qi}^2 \phi_{qi}^2 q_{ei}^2}{4b_{qi}} + b_{qi} = \frac{\sigma_{qi} \Phi_{qi} q_{ei}^2}{(1 + \varsigma_{qi} \xi_q) m_{qi}} + b_{qi} \end{aligned} \quad (24)$$

where $\Phi_{ui} = \phi_{ui}^2/(4b_{ui})$, $\Phi_{qi} = \phi_{qi}^2/(4b_{qi})$. b_{ui} and b_{qi} denote the positive constants. $\sigma_{ui} = (1 + \varsigma_{ui}\xi_u)m_{ui}\Xi_{ui}^2$ and $\sigma_{qi} = (1 + \varsigma_{qi}\xi_q)m_{qi}\Xi_{qi}^2$ indicate the unknown adaptive parameters, which will be compensated by the adaptive laws designed in the following process. Therefore, according to (17), (22), (23) and (24), the derivative of kinetic errors can be expressed as

$$\begin{aligned}\dot{u}_{ei} &\leq -\frac{\zeta_{ui}}{t_{ui}} + \frac{\sigma_{ui}\Phi_{ui}u_{ei}}{(1+\varsigma_{ui}\xi_u)m_{ui}} - \frac{1}{(1+\varsigma_{ui}\xi_u)m_{ui}}\tilde{u}_{ui} + b_{ui} \\ \dot{q}_{ei} &\leq -\frac{\zeta_{qi}}{t_{qi}} + \frac{\sigma_{qi}\Phi_{qi}q_{ei}}{(1+\varsigma_{qi}\xi_q)m_{qi}} - \frac{1}{(1+\varsigma_{qi}\xi_q)m_{qi}}\tilde{q}_{qi} + b_{qi}\end{aligned}\quad (25)$$

To facilitate the expression, one defines $\bar{m}_{ui} = (1 + \varsigma_{ui}\xi_u)m_{ui}$ and $\bar{m}_{qi} = (1 + \varsigma_{qi}\xi_q)m_{qi}$. To stabilize the kinetic errors, the control input variables \tilde{u}_{ui} and \tilde{q}_{qi} are designed as

$$\begin{aligned}\tilde{u}_{ui} &= k_{ui}u_{ei} - \frac{\zeta_{ui}}{t_{ui}} + \hat{\sigma}_{ui}\Phi_{ui}u_{ei} \\ \tilde{q}_{qi} &= k_{qi}q_{ei} - \frac{\zeta_{qi}}{t_{qi}} + \hat{\sigma}_{qi}\Phi_{qi}q_{ei}\end{aligned}\quad (26)$$

where k_{ui} and k_{qi} denote the positive control parameters set by user. To compensate the unknown terms during the stability analysis, the adaptive updating parameters $\hat{\sigma}_{ui}$ and $\hat{\sigma}_{qi}$ are derived as

$$\begin{aligned}\dot{\hat{\sigma}}_{ui} &= \gamma_{ui} \left[\Phi_{ui}u_{ei}^2 - \delta_{ui}(\hat{\sigma}_{ui} - \hat{\sigma}_{ui}(0)) \right] \\ \dot{\hat{\sigma}}_{qi} &= \gamma_{qi} \left[\Phi_{qi}q_{ei}^2 - \delta_{qi}(\hat{\sigma}_{qi} - \hat{\sigma}_{qi}(0)) \right]\end{aligned}\quad (27)$$

where γ_{ui} , γ_{qi} , δ_{ui} and δ_{qi} indicate the adaptive control parameters. $\hat{\sigma}_{ui}$ and $\hat{\sigma}_{qi}$ are the estimated variables of σ_{ui} and σ_{qi} with $\tilde{\sigma}_{ui} = \hat{\sigma}_{ui} - \sigma_{ui}$, $\tilde{\sigma}_{qi} = \hat{\sigma}_{qi} - \sigma_{qi}$.

C. Stability Analysis of Closed-Loop System

In this section, the stability analysis of the AUV closed-loop system can be demonstrated as Theorem 1. The minimum triggering interval time of the proposed DCETM will be proved to avoid the Zeno behavior.

Theorem 1: Suppose that all signals in the closed-loop system are defined in a compact set, i.e., $\Omega_0 = \{\check{\chi}_{ei}^2(0) + \check{\theta}_{ei}^2(0) + u_{ei}^2(0) + q_{ei}^2(0) + \zeta_{ui}(0)^2 + \zeta_{qi}(0)^2 + \tilde{\sigma}_{ui}^2(0) + \tilde{\sigma}_{qi}^2(0) \leq \epsilon\}$ with any $\epsilon > 0$. Considering the AUV closed-loop system (1), (2) under Assumption 1-3 with the triggering conditions of DCETM (13), (15), the virtual control laws (19), the DSC filters (20), the one-parameter integrated learning method (23), the controllers (26) and the adaptive laws (27), the signals in the closed-loop system are guaranteed to exhibit SGUUB stability, ensuring that both the position error $\check{\chi}_{ei}$ and the orientation error $\check{\theta}_{ei}$ will be closed to a compact set. Finally, the Zeno behavior will be mathematically excluded.

Proof: First, the Lyapunov function is constructed as

$$V = \sum_{i=1}^N \left\{ \frac{1}{2}\check{\chi}_{ei}^2 + \frac{1}{2}\check{\theta}_{ei}^2 + \frac{1}{2}u_{ei}^2 + \frac{1}{2}q_{ei}^2 + \frac{1}{2}\zeta_{ui}^2 + \frac{1}{2}\zeta_{qi}^2 + \frac{1}{2\bar{m}_{ui}\gamma_{ui}}\tilde{\sigma}_{ui}^2 + \frac{1}{2\bar{m}_{qi}\gamma_{qi}}\tilde{\sigma}_{qi}^2 \right\} \quad (28)$$

Then, the derivative of the Lyapunov function can be expressed as

$$\dot{V} = \sum_{i=1}^N \left\{ \check{\chi}_{ei}\dot{\check{\chi}}_{ei} + \check{\theta}_{ei}\dot{\check{\theta}}_{ei} + u_{ei}\dot{u}_{ei} + q_{ei}\dot{q}_{ei} + \zeta_{ui}\dot{\zeta}_{ui} + \zeta_{qi}\dot{\zeta}_{qi} + \bar{m}_{ui}^{-1}\gamma_{ui}^{-1}\tilde{\sigma}_{ui}\dot{\tilde{\sigma}}_{ui} + \bar{m}_{qi}^{-1}\gamma_{qi}^{-1}\tilde{\sigma}_{qi}\dot{\tilde{\sigma}}_{qi} \right\} \quad (29)$$

By substituting (18), (19), (25) into (29), one can obtain

$$\begin{aligned}\dot{V} &\leq \sum_{i=1}^N \left\{ (1 + \varsigma_{\chi i}\xi_{\chi}) \left[-k_{\chi i}\check{\chi}_{ei}^2 + \zeta_{ui}\check{\chi}_{ei} + u_{ei}\check{\chi}_{ei} \right] \right. \\ &\quad + (1 + \varsigma_{\theta i}\xi_{\theta}) \left[-k_{\theta i}\check{\theta}_{ei}^2 + \zeta_{qi}\check{\theta}_{ei} + q_{ei}\check{\theta}_{ei} \right] \\ &\quad - \frac{\zeta_{ui}}{t_{ui}}u_{ei} + \frac{\sigma_{ui}\Phi_{ui}u_{ei}^2}{(1+\varsigma_{ui}\xi_u)m_{ui}} - \frac{u_{ei}\tilde{u}_{ui}}{(1+\varsigma_{ui}\xi_u)m_{ui}} \\ &\quad - \frac{\zeta_{qi}}{t_{qi}}q_{ei} + \frac{\sigma_{qi}\Phi_{qi}q_{ei}^2}{(1+\varsigma_{qi}\xi_q)m_{qi}} - \frac{q_{ei}\tilde{q}_{qi}}{(1+\varsigma_{qi}\xi_q)m_{qi}} \\ &\quad + \zeta_{ui}\dot{\zeta}_{ui} + \zeta_{qi}\dot{\zeta}_{qi} + b_{ui} + b_{qi} + \bar{m}_{ui}^{-1}\gamma_{ui}^{-1}\tilde{\sigma}_{ui}\dot{\tilde{\sigma}}_{ui} \\ &\quad \left. + \bar{m}_{qi}^{-1}\gamma_{qi}^{-1}\tilde{\sigma}_{qi}\dot{\tilde{\sigma}}_{qi} \right\}\end{aligned}\quad (30)$$

To facilitate the following analysis, the Young's inequality is useful. By combining with (20) and (21), we have

$$\zeta_{ui}\check{\chi}_{ei} \leq \frac{\zeta_{ui}^2}{2} + \frac{\check{\chi}_{ei}^2}{2}, \quad \zeta_{qi}\check{\theta}_{ei} \leq \frac{\zeta_{qi}^2}{2} + \frac{\check{\theta}_{ei}^2}{2} \quad (31)$$

$$u_{ei}\check{\chi}_{ei} \leq \frac{u_{ei}^2}{2} + \frac{\check{\chi}_{ei}^2}{2}, \quad q_{ei}\check{\theta}_{ei} \leq \frac{q_{ei}^2}{2} + \frac{\check{\theta}_{ei}^2}{2} \quad (32)$$

$$\begin{aligned}\zeta_{ui}\dot{\zeta}_{ui} &= -\frac{\zeta_{ui}^2}{t_{ui}} - \zeta_{ui}\dot{\alpha}_{ui} \leq -\frac{\zeta_{ui}^2}{t_{ui}} + \frac{\zeta_{ui}^2 B_{ui}^2(\cdot) M_{ui}^2}{4a_{ui} M_{ui}^2} + a_{ui} \\ &\leq -\left(\frac{1}{t_{ui}} - \frac{M_{ui}^2}{4a_{ui}} \right) \zeta_{ui}^2 + a_{ui}, \quad \iota = u, q\end{aligned}\quad (33)$$

Due to the property of $\varsigma_{\chi i}, \varsigma_{\theta i} \in [-1, 1]$ and ξ_{χ}, ξ_{θ} always setting in $(0, 1]$, by substituting (26) and (31)-(33), the derivative of V can be further expressed as

$$\begin{aligned}\dot{V} &\leq \sum_{i=1}^N \left\{ -2(k_{\chi i} - 1)\check{\chi}_{ei}^2 - 2(k_{\theta i} - 1)\check{\theta}_{ei}^2 \right. \\ &\quad - \left(\frac{1}{t_{ui}} - 1 - \frac{M_{ui}^2}{4a_{ui}} \right) \zeta_{ui}^2 - \left(\frac{1}{t_{qi}} - 1 - \frac{M_{qi}^2}{4a_{qi}} \right) \zeta_{qi}^2 \\ &\quad - \left(\frac{k_{ui}}{\bar{m}_{ui}} - 1 \right) u_{ei}^2 - \left(\frac{k_{qi}}{\bar{m}_{qi}} - 1 \right) q_{ei}^2 \\ &\quad + \left(\frac{1}{\bar{m}_{ui}} - 1 \right) \frac{\zeta_{ui}}{t_{ui}} u_{ei} + \left(\frac{1}{\bar{m}_{qi}} - 1 \right) \frac{\zeta_{qi}}{t_{qi}} q_{ei} \\ &\quad - \frac{\tilde{\sigma}_{ui}\Phi_{ui}u_{ei}^2}{\bar{m}_{ui}} - \frac{\tilde{\sigma}_{qi}\Phi_{qi}q_{ei}^2}{\bar{m}_{qi}} + a_{ui} + a_{qi} + b_{ui} + b_{qi} \\ &\quad \left. + \bar{m}_{ui}^{-1}\gamma_{ui}^{-1}\tilde{\sigma}_{ui}\dot{\tilde{\sigma}}_{ui} + \bar{m}_{qi}^{-1}\gamma_{qi}^{-1}\tilde{\sigma}_{qi}\dot{\tilde{\sigma}}_{qi} \right\}\end{aligned}\quad (34)$$

According to (34), we can obtain the following inequalities

$$\begin{aligned}\left(\frac{1}{\bar{m}_{ui}} - 1 \right) \frac{\zeta_{ui}}{t_{ui}} u_{ei} &\leq \frac{1 + \frac{1}{\bar{m}_{ui}}}{2t_{ui}} \zeta_{ui}^2 + \frac{1 + \frac{1}{\bar{m}_{ui}}}{2t_{ui}} u_{ei}^2 \\ \left(\frac{1}{\bar{m}_{qi}} - 1 \right) \frac{\zeta_{qi}}{t_{qi}} q_{ei} &\leq \frac{1 + \frac{1}{\bar{m}_{qi}}}{2t_{qi}} \zeta_{qi}^2 + \frac{1 + \frac{1}{\bar{m}_{qi}}}{2t_{qi}} q_{ei}^2\end{aligned}\quad (35)$$

In conjunction with (27), (35), the derivative of V (34) can be rewritten as

$$\begin{aligned} \dot{V} \leq & \sum_{i=1}^N \left\{ -2(k_{\chi i} - 1)\check{\chi}_{ei}^2 - 2(k_{\theta i} - 1)\check{\theta}_{ei}^2 \right. \\ & - \left(\frac{1}{t_{ui}} - 1 - \frac{M_{ui}^2}{4a_{ui}} - \frac{1 + \frac{1}{\bar{m}_{ui}}}{2t_{ui}} \right) \zeta_{ui}^2 \\ & - \left(\frac{1}{t_{qi}} - 1 - \frac{M_{qi}^2}{4a_{qi}} - \frac{1 + \frac{1}{\bar{m}_{qi}}}{2t_{qi}} \right) \zeta_{qi}^2 \\ & - \left(\frac{k_{ui}}{\bar{m}_{ui}} - 1 - \frac{1 + \frac{1}{\bar{m}_{ui}}}{2t_{ui}} \right) u_{ei}^2 - \left(\frac{k_{qi}}{\bar{m}_{qi}} - 1 - \frac{1 + \frac{1}{\bar{m}_{qi}}}{2t_{qi}} \right) q_{ei}^2 \\ & - \frac{\delta_{ui}}{2\bar{m}_{ui}} \tilde{\sigma}_{ui}^2 - \frac{\delta_{qi}}{2\bar{m}_{qi}} \tilde{\sigma}_{qi}^2 + a_{ui} + a_{qi} + b_{ui} + b_{qi} \\ & \left. + \frac{\delta_{ui}}{2\bar{m}_{ui}} (\sigma_{ui} - \hat{\sigma}_{ui}(0))^2 + \frac{\delta_{qi}}{2\bar{m}_{qi}} (\sigma_{qi} - \hat{\sigma}_{qi}(0))^2 \right\} \quad (36) \end{aligned}$$

Define $\kappa = \min\{2k_{\chi i} - 2, 2k_{\theta i} - 2, 1/t_{ui} - 1 - M_{ui}^2/(4a_{ui}) - (1 + 1/\bar{m}_{ui})/(2t_{ui}), 1/t_{qi} - 1 - M_{qi}^2/(4a_{qi}) - (1 + 1/\bar{m}_{qi})/(2t_{qi}), k_{ui}/\bar{m}_{ui} - 1 - (1 + 1/\bar{m}_{ui})/(2t_{ui}), k_{qi}/\bar{m}_{qi} - 1 - (1 + 1/\bar{m}_{qi})/(2t_{qi}), \delta_{ui}\gamma_{ui}/(2\bar{m}_{ui}), \delta_{qi}\gamma_{qi}/(2\bar{m}_{qi})\}$. Then, we have

$$\dot{V} \leq -2\kappa V + \varrho \quad (37)$$

where $\varrho = \sum_{i=1}^N \{a_{ui} + a_{qi} + b_{ui} + b_{qi} + \delta_{ui}/(2\bar{m}_{ui})(\sigma_{ui} - \hat{\sigma}_{ui}(0))^2 + \delta_{qi}/(2\bar{m}_{qi})(\sigma_{qi} - \hat{\sigma}_{qi}(0))^2\}$. Let $\kappa > \varrho/(2\epsilon)$, then $\dot{V} \leq -2\kappa V + \varrho$ holds for any initial states in Ω_0 and all $t \geq 0$. Then, $V(t) \leq \varrho/(2\kappa) + (V(0) - \varrho/(2\kappa))\exp(-2\kappa t)$ can be obtained by the integrated of (37). According to Lemma 1, it is implied that all signals in the closed-loop control system are with SGUUB stability. Since $\lim_{t \rightarrow \infty} |\check{\chi}_{ei}(t)| \leq (\varrho/(2\kappa))^{1/2} < \sqrt{\epsilon}$ and $\lim_{t \rightarrow \infty} |\check{\theta}_{ei}(t)| \leq (\varrho/(2\kappa))^{1/2} < \sqrt{\epsilon}$, it is concluded that the tracking errors of AUVs can converge to a small residual set.

In the following, one will demonstrate the proposed DCETM can effectively exclude the Zeno behavior, i.e., there exists a positive number $t^* > 0$ such that the inter-sampling interval $\{t_{k+1} - t_k\} \geq t^*, \forall k \in \mathbb{Z}^+$. Considering $e_{xi} = \check{x}_{ei}(t) - x_{ei}(t)$, $e_{zi} = \check{z}_{ei}(t) - z_{ei}(t)$, $\forall t \in [t^*, t_{k+1,i}^*)$, $e_{\theta i} = \check{\theta}_{ei}(t) - \theta_{ei}(t)$, $\forall t \in [t^*, t_{k+1,i}^*)$, the following result holds for the triggering condition 1:

$$\begin{aligned} \frac{d}{dt}|e_{xi}| &= \frac{d}{dt}(e_{xi} * e_{xi})^{\frac{1}{2}} = \text{sgn}(e_{xi})\dot{e}_{xi} \leq |\dot{\check{x}}_{ei}(t)| \\ \frac{d}{dt}|e_{zi}| &= \frac{d}{dt}(e_{zi} * e_{zi})^{\frac{1}{2}} = \text{sgn}(e_{zi})\dot{e}_{zi} \leq |\dot{\check{z}}_{ei}(t)| \\ \frac{d}{dt}|e_{\theta i}| &= \frac{d}{dt}(e_{\theta i} * e_{\theta i})^{\frac{1}{2}} = \text{sgn}(e_{\theta i})\dot{e}_{\theta i} \leq |\dot{\check{\theta}}_{ei}(t)| \quad (38) \end{aligned}$$

From (17), $\check{x}_{ei}(t)$, $\check{z}_{ei}(t)$ and $\check{\theta}_{ei}(t)$ are differentiable and $\dot{\check{x}}_{ei}(t)$, $\dot{\check{z}}_{ei}(t)$ and $\dot{\check{\theta}}_{ei}(t)$ are the functions about the bounded signals of the closed-loop systems. Thus, we can find positive constants $\epsilon_x > 0$, $\epsilon_z > 0$ and $\epsilon_\theta > 0$ such that $|\dot{\check{x}}_{ei}(t)| \leq \epsilon_x$, $|\dot{\check{z}}_{ei}(t)| \leq \epsilon_z$ and $|\dot{\check{\theta}}_{ei}(t)| \leq \epsilon_\theta$. For $e_{xi}(t_{k,i}^*) = 0$, $e_{zi}(t_{k,i}^*) = 0$ and $e_{\theta i}(t_{k,i}^*) = 0$ while

TABLE I

THE FORMULA SUMMARIZATION OF THE PROPOSED CONTROL SCHEME

Repulsive Force Fields of MAPF	
$U_{att1} = \frac{1}{2}k_{att1}\rho_{ia}^2$	$U_{att2} = \frac{1}{2}k_{att2}\rho_{ic}^2$
$U_{rep1} = \frac{1}{2}k_{rep1}\left(\frac{1}{\rho_{io}} - \frac{1}{d_o}\right)\rho_{ia}^2$	$U_{rep2} = \frac{1}{2}k_{rep2}\left(\frac{1}{\rho_{ij}} - \frac{1}{2R}\right)\rho_{ic}^2$
Desired Guidance Signals	
$\dot{x}_d = u_d \cos \theta_F - w_d \sin \theta_F$, $\dot{z}_d = u_d \sin \theta_F + w_d \cos \theta_F$	
$\theta_d = 0.5\text{sgn}(z_d - z_i)\pi[1 - \text{sgn}(x_d - x_i)] + \arctan\left(\frac{z_d - z_i}{x_d - x_i}\right)$	
Triggering Conditions of DCETM	
$t_{k+1,i}^x = \inf\left\{t > t_{k,i}^x \mid e_{xi} \geq \xi_\chi x_{ei}(t) \wedge e_{zi} \geq \xi_\chi z_{ei}(t) \right\}$	
$t_{k+1,i}^\theta = \inf\left\{t > t_{k,i}^\theta \mid e_{\theta i} \geq \xi_\theta \theta_{ei}(t) \right\}$	
$t_{k+1,i}^u = \inf\left\{t > t_{k,i}^u \mid e_{ui}(t) \geq \xi_u \tau_{ui}(t) \right\}$	
$t_{k+1,i}^q = \inf\left\{t > t_{k,i}^q \mid e_{qi}(t) \geq \xi_q \tau_{qi}(t) \right\}$	
Control Signal Transformation	
$x_{ei}(t) = \check{x}_{ei}(t_{k,i}^x)$, $z_{ei}(t) = \check{z}_{ei}(t_{k,i}^x)$, $\forall t \in [t_{k,i}^x, t_{k+1,i}^x)$	
$\theta_{ei}(t) = \check{\theta}_{ei}(t_{k,i}^\theta)$, $\forall t \in [t_{k,i}^\theta, t_{k+1,i}^\theta)$	
$\tau_{ui}(t) = \check{\tau}_{ui}(t_{k,i}^u)$, $\forall t \in [t_{k,i}^u, t_{k+1,i}^u)$	
$\tau_{qi}(t) = \check{\tau}_{qi}(t_{k,i}^q)$, $\forall t \in [t_{k,i}^q, t_{k+1,i}^q)$	
Kinematic Virtual Control Laws	
$\alpha_{ui} = \frac{1}{\cos \theta_{ei}}(-k_{\chi i}\check{\chi}_{ei} + \dot{x}_d \cos \theta_d + \dot{z}_d \sin \theta_d - w_i \sin \theta_{ei})$	
$\alpha_{qi} = k_{\theta i}\check{\theta}_{ei} + \dot{\theta}_d$	
DSC Filters	
$t_{ui}\beta_{ui} + \beta_{ui} = \alpha_{ui}$, $\beta_{ui}(0) = \alpha_{ui}(0)$	
$t_{qi}\beta_{qi} + \beta_{qi} = \alpha_{qi}$, $\beta_{qi}(0) = \alpha_{qi}(0)$	
Kinetic Final Control Laws	
$\check{\tau}_{ui} = k_{ui}u_{ei} - \frac{\zeta_{ui}}{t_{ui}} + \hat{\sigma}_{ui}\Phi_{ui}u_{ei}$	
$\check{\tau}_{qi} = k_{qi}q_{ei} - \frac{\zeta_{qi}}{t_{qi}} + \hat{\sigma}_{qi}\Phi_{qi}q_{ei}$	
Adaptive Laws	
$\dot{\hat{\sigma}}_{ui} = \gamma_{ui}[\Phi_{ui}u_{ei}^2 - \delta_{ui}(\hat{\sigma}_{ui} - \hat{\sigma}_{ui}(0))]$	
$\dot{\hat{\sigma}}_{qi} = \gamma_{qi}[\Phi_{qi}q_{ei}^2 - \delta_{qi}(\hat{\sigma}_{qi} - \hat{\sigma}_{qi}(0))]$	

$\lim_{t \rightarrow t_{k+1,i}^x} e_{xi}(t) = \xi_\chi |x_{ei}| > 0$, $\lim_{t \rightarrow t_{k+1,i}^x} e_{zi}(t) = \xi_\chi |z_{ei}| > 0$ and $\lim_{t \rightarrow t_{k+1,i}^\theta} e_{\theta i}(t) = \xi_\theta |\theta_{ei}| > 0$, the lower bound of t^* for triggering condition 1 can be represented as $t^* \geq \max\{(\xi_\chi |x_{ei}|)/\epsilon_x, (\xi_\chi |z_{ei}|)/\epsilon_z, (\xi_\theta |\theta_{ei}|)/\epsilon_\theta\}$.

Similarly, due to $e_{ui} = \check{\tau}_{ui}(t) - \tau_{ui}(t)$, $\forall t \in [t^*, t_{k+1,i}^u)$, and $e_{qi} = \check{\tau}_{qi}(t) - \tau_{qi}(t)$, $\forall t \in [t^*, t_{k+1,i}^q)$, we know that $\frac{d}{dt}|e_{ui}| \leq |\dot{\check{\tau}}_{ui}(t)|$ and $\frac{d}{dt}|e_{qi}| \leq |\dot{\check{\tau}}_{qi}(t)|$ hold for the triggering condition 2. Due to $\check{\tau}_{ui}(t)$, $\check{\tau}_{qi}(t)$ are differentiable and $\check{\tau}_{ui}(t)$, $\check{\tau}_{qi}(t)$ are bounded, it is obvious that there exist the positive constants $\epsilon_u > 0$, $\epsilon_q > 0$ satisfying $|\dot{\check{\tau}}_{ui}(t)| \leq \epsilon_u$ and $|\dot{\check{\tau}}_{qi}(t)| \leq \epsilon_q$. According to the triggering condition, we know $e_{ui}(t_{k,i}^u) = 0$, $e_{qi}(t_{k,i}^q) = 0$ and $\lim_{t \rightarrow t_{k+1,i}^u} e_{ui}(t) = \xi_u |\tau_{ui}| > 0$, $\lim_{t \rightarrow t_{k+1,i}^q} e_{qi}(t) = \xi_q |\tau_{qi}| > 0$. So, the lower bound of t^* for triggering condition 2 is $t^* \geq \max\{(\xi_u |\tau_{ui}|)/\epsilon_u, (\xi_q |\tau_{qi}|)/\epsilon_q\}$. Finally, the lower bound of the inter-sampling intervals t^* must satisfy $t^* \geq \max\{(\xi_\chi |x_{ei}|)/\epsilon_x, (\xi_\chi |z_{ei}|)/\epsilon_z, (\xi_\theta |\theta_{ei}|)/\epsilon_\theta, (\xi_u |\tau_{ui}|)/\epsilon_u, (\xi_q |\tau_{qi}|)/\epsilon_q\} > 0$. Based on above discussion, the Zeno behavior of the proposed DCETM can be successfully excluded. The proof is finished. \square

Remark 1: In this paper, the MAPF algorithm is proposed for AUVs to achieve the obstacles avoidance and safety navigation under the multiple obstacles environment. Different from the traditional APF method designed for a single AUV [14], the framework incorporates distinct potential fields for the guidance. To be specific, the attractive field,

denotes as U_{att1} , steers the AUVs towards the desired position, while U_{att2} is employed to prevent the formation splitting when an AUV deviates from the center of the formation configuration. For the repulsive force field, U_{rep1} serves as a repulsive field to prevent collisions of external obstacles, and U_{rep2} is specifically designed for the collision among the AUVs. Therefore, the MAPF planning algorithm facilitates the achievement of collision-free path tracking and successful completion of formation splitting prevention missions.

Remark 2: Compared to the existing ETC methods [24], [25], [26], [27], [28], [29], [30], [31], [32], the proposed DCETM proposed in (13)-(16) offers an efficient solution to economize both the S-C and C-A channels. This enables a balance between tracking accuracy and communication channel utilization. When the triggering condition for S-C channel (13) is activated, the feedback errors are transmitted to the controller only at the trigger point, effectively reducing sensor usage frequency. Conversely, when the triggering condition for the C-A channel (15) is triggered, the control laws (26) only actuate the actuators at the trigger point, mitigating the issue of frequent actuator execution.

Remark 3: During the control process, a one-parameter integrated learning scheme (23) is utilized to reduce the computational burden associated with updating the weights of the FS. Consequently, each control channel, represented by $\tilde{\tau}_{ui}$ and $\tilde{\tau}_{qi}$ in (26), only requires a single adaptive parameter, i.e., $\hat{\sigma}_{ui}$ or $\hat{\sigma}_{qi}$, for online updates. This approach eliminates the need to update entire weight vectors Θ_{ui} , Θ_{qi} , resulting in reduced computational complexity and concise control laws. In addition, it is worth noting that ϕ_{ui} , ϕ_{qi} are related to $S_{ui}(\mathbf{v})$, $S_{qi}(\mathbf{v})$, while Φ_{ui} , Φ_{qi} exhibit a quadratic relationship with ϕ_{ui} , ϕ_{qi} , which means that the parameters Φ_{ui} , Φ_{qi} are relevant to FS employed in (26) and (27).

V. SIMULATION RESULTS

In this section, three simulation examples are provided to verify the effectiveness of the proposed control algorithm: the simulation example in a multiple obstacles environment, the simulation example in varying water depths and the comparative simulation example. The underactuated AUV model in [8] and [37] is chosen to be the experimental objective. The model parameters are set as $m_{11} = 200\text{kg}$, $m_{22} = 250\text{kg}$, $m_{33} = 80\text{kg}$, $d_{11} = (70 + 100|u|)\text{kg/s}$, $d_{22} = (100 + 200|w|)\text{kg/s}$ and $d_{33} = (50 + 100|q|)\text{kg/s}$. Considering the effect caused by ocean current, the nonlinear functions are adopted to simulate the unknown sea loads, which can be established as: $\tau_{su} = 0.1 \sin(t) + 0.05 \sin(\pi t) + d_{su}$, $\tau_{sw} = 0.1 \cos(\pi t) + d_{sw}$ and $\tau_{sq} = 0.1 \sin(\pi t) + d_{sq}$. The first-order Markov process of (39) is employed to describe the coupling of high and low frequency components of the ocean current.

$$\begin{cases} \dot{d}_{su} = -d_{su} + 0.05\omega_u \\ \dot{d}_{sw} = -d_{sw} + 0.05\omega_w \\ \dot{d}_{sq} = -d_{sq} + 0.05\omega_q \end{cases} \quad (39)$$

where ω_u , ω_w and ω_q are three independent white noise variables with the variance of 1. Compared with the sinusoidal waves, it is more authentic to simulate the effect of the external

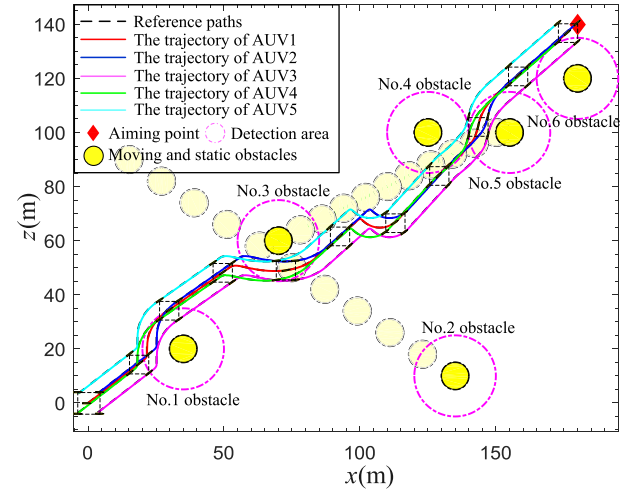


Fig. 4. The trajectories of five AUVs under the multiple obstacles environment by using the MAPF planning method.

interference [15]. In the following, we will provide the three simulation examples in detail.

A. The Simulation Example With Multiple Obstacles Environment

To demonstrate the effectiveness of the MAPF planning method and the proposed control algorithm, we carry out the simulation in a complex environment with multiple obstacles. Six moving/static obstacles are set near or crossing the reference path to impose navigational difficulty for AUVs. Their central coordinates are chosen as: (35m, 20m), (15m, 90m), (150m, 100m), (125m, 100m), (155m, 100m), (180m, 120m), respectively. It is noted that the No.1, No.4, No.5 and No.6 obstacles are static, while the No.2 and No.3 obstacles are moving with the speed (0.3m/s, -0.2m/s), (-0.2m/s, -0.1m/s), respectively.

To constitute the formation, five AUVs are arranged in a rectangular configuration with specified ranges and relative angles: $\Delta_1 = [0, 0, 0]^T$, $\Delta_2 = [5 \sin(\frac{\pi}{4}), 5 \cos(\frac{\pi}{4}), 0]^T$, $\Delta_3 = [5 \sin(\frac{3\pi}{4}), 5 \cos(\frac{3\pi}{4}), 0]^T$, $\Delta_4 = [5 \sin(\frac{5\pi}{4}), 5 \cos(\frac{5\pi}{4}), 0]^T$, $\Delta_5 = [7 \sin(\frac{\pi}{4}), 7 \cos(\frac{\pi}{4}), 0]^T$, respectively. Initial conditions of five AUVs are set as: $\eta_1(t_0) = [0\text{m}, 0\text{m}, 0\text{deg}]^T$, $\eta_2(t_0) = [4\text{m}, 4\text{m}, 0\text{deg}]^T$, $\eta_3(t_0) = [4\text{m}, -4\text{m}, 0\text{deg}]^T$, $\eta_4(t_0) = [-4\text{m}, -4\text{m}, 0\text{deg}]^T$, $\eta_5(t_0) = [-4\text{m}, 4\text{m}, 0\text{deg}]^T$, respectively. The initial velocities of all the AUVs are $\mathbf{v}_i = [0\text{m/s}, 0\text{m/s}, 0\text{rad/s}]^T$, $i = 1, \dots, 5$. The initial condition of virtual underwater vehicle is set as $\eta_d(t_0) = [0\text{m}, -4\text{m}, 0\text{deg}]^T$. The central coordinate of the aiming point is (180m, 140m), which is marked by the red diamond in Fig. 4. The parameters of the control scheme are set as $k_{\chi i} = 2.5$, $k_{\theta i} = 1.2$, $k_{ui} = 170$, $k_{qi} = 100$, $k_{att1i} = 1$, $k_{att2i} = 1$, $k_{rep1i} = 10$, $k_{rep2i} = 10$, $d_o = 15\text{m}$, $R = 1\text{m}$, $\xi_{\chi i} = 0.01$, $\xi_{\theta i} = 0.02$, $\xi_{ui} = 0.08$, $\xi_{qi} = 0.28$, $t_{ui} = t_{qi} = 0.01$, $\gamma_{ui} = \gamma_{qi} = 1.2$, $b_{ui} = b_{qi} = 4.3$, $\delta_{ui} = \delta_{qi} = 4.5$, $i = 1, \dots, 5$.

Remark 4: The designed parameters are adjusted using a trial-and-error strategy. Taking control parameters as an example, it is important to ensure that the gain parameters are sufficiently large to achieve good control performance.

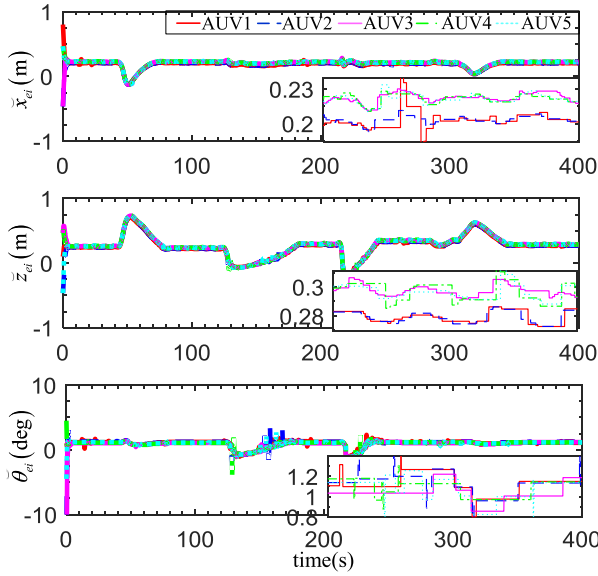


Fig. 5. The curve of the attitude errors with DCETM.

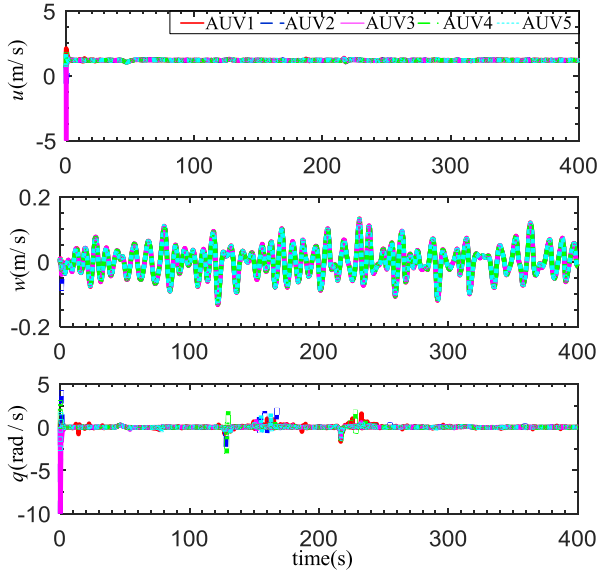


Fig. 6. The curve of the velocity.

However, setting parameters too large can result in unexpectedly large control signals. Therefore, the initial approach is to set relatively larger values for the gain parameters, such as k_{χ_i} , k_{θ_i} , k_{u_i} , k_{q_i} , \dots , δ_{u_i} , δ_{q_i} . Subsequently, the parameters are reasonably reduced through simulation tests. This iterative process ensures the effectiveness of parameter settings in practical engineering.

The main simulated results are provided in Fig. 4-Fig. 8. Figure 4 shows the trajectories of AUVs formation navigating in a challenging environment with various obstacles, including both moving and static obstacles. To increase the complexity of the navigation environment, the crossing situation (No.2 obstacle) and the head-on situation (No.3 obstacle) are occurred in about 120s and 220s, and other four static obstacles are also set near the reference path. From Fig. 4, it is apparent that by virtue of the proposed MAPF planning algorithm, the AUVs can sail along the reference path toward

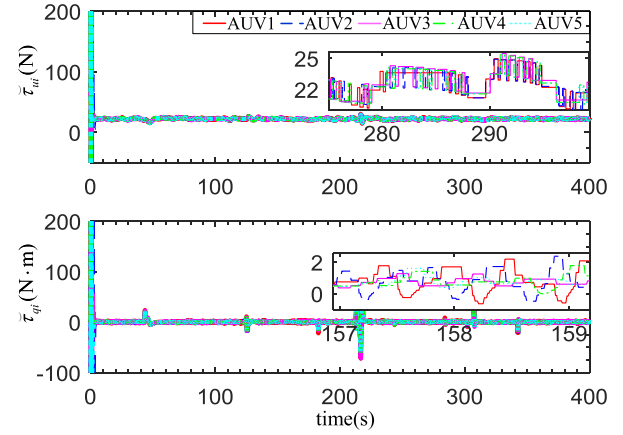


Fig. 7. The curve of the control input with DCETM.

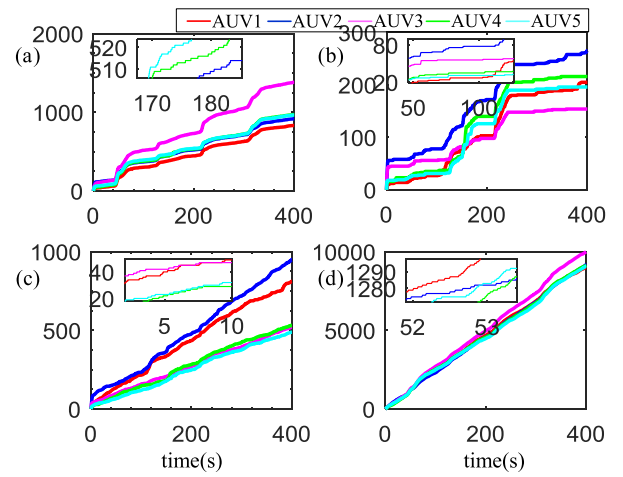


Fig. 8. Accumulation of the triggering times.

to the aiming point and evade the various obstacles without the formation splitting. In Fig. 5, the curve of the attitude errors of five AUVs is exhibited. It is worth noting that the curves of kinematic error variables \check{x}_{ei} , \check{z}_{ei} and $\check{\theta}_{ei}$ parent a stair-stepping form, indicating that the signals are only transmitted to the controller at the triggering instant by virtue of the proposed DCETM. That effectively reduces the communication burden in the S-C channel. Although the corresponding curves exist some fluctuations around 50s, 120s, 220s, 300s, it is a reasonable phenomenon due to the AUV formation avoiding obstacles. Figure 6 describes the curve of velocity variables. It is clear that the velocity variables can be stabilized in a bounded range, which implies the corresponding signals are bounded in the closed-loop system. Figure 7 illustrates the control input curves for the five AUVs. It is evident that the control signals, generated by the event-triggered fuzzy control laws in real-time, are only transmitted to the actuators at the triggering instant. Despite the influence of unknown sea loads, the control inputs are with the little joggle benefiting from the DCETM. In Fig. 8, the accumulation of triggering instants of five AUVs with the DCETM is exhibited. To be specific, Fig. 8(a) shows the accumulation of triggering instants $t_{k,i}^x$ in first formula of triggering condition for S-C channel (13), while Fig. 8(b) represents the accumulation of $t_{k,i}^\theta$ in second

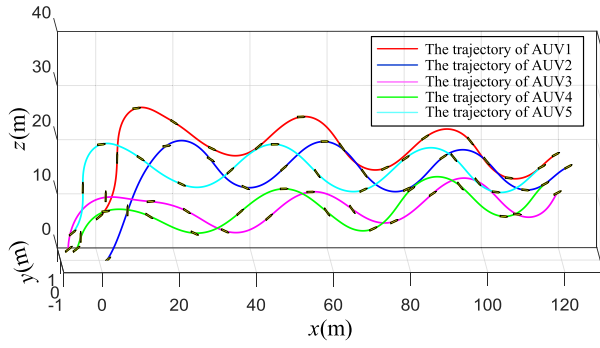


Fig. 9. The trajectories of five AUVs under varying water depth.

formula of (13). Likewise, Fig. 8(c) exhibits the accumulation of $t_{k,i}^u$ in first formula of triggering condition for C-A channel (15), while Fig. 8(d) represents the accumulation of $t_{k,i}^\theta$ in second formula of (13). Compared to the traditional time-triggering control scheme, which uses 40000 sampling instances (with a simulated time step of 0.01s), the proposed scheme significantly reduces the pressure on signal transmission and bandwidth utilization in both the S-C and C-A channels.

B. The Simulation Example Under the Varying Water Depth

To verify the effectiveness of the proposed scheme, the simulation example has been developed under varying water depth conditions. The reference of η_d is described as $x_d(t) = t$, $z_d(t) = 15 \exp(-0.01t) \sin(\pi t/20) + 15$, $\theta_d(t) = \arctan[0.15 \exp(-0.01t) \sin(\pi t/20) - 3\pi/4 \exp(-0.01t) \cos(\pi t/20)]$. The desired configuration is chosen as a shrunk pentagon formation. Initial conditions of five AUVs are set as: $\eta_1(t_0) = [0m, 8m, \pi/6rad]^T$, $\eta_2(t_0) = [2m, 0m, \pi/4rad]^T$, $\eta_3(t_0) = [-8m, 2m, \pi/2rad]^T$, $\eta_4(t_0) = [-6m, 2m, \pi/5rad]^T$, $\eta_5(t_0) = [-7m, 5m, \pi/5rad]^T$, respectively. The corresponding parameters setting and remainder states setting are the same as the Section V-A. Then, the numerical experiment is carried out.

Figure 9 shows the trajectories of five AUVs under the varying water depth. With the proposed control scheme, it is evident that five AUVs can sail along the reference path while maintaining the desired configuration. Figure 10 describes the tracking errors curves of five AUVs. Although the curves fluctuates in the varying water depth environment, the relevant error variables of AUVs remain stable in a small range. From the local zoom detail of Fig. 10, we can found that the corresponding errors \tilde{x}_{ei} , \tilde{z}_{ei} and $\tilde{\theta}_{ei}$ of AUVs are updated only at the triggering point during the deep sea operation, which demonstrates the effectiveness of the triggering condition in (13). Figure 11 provides the curve of velocities under the varying water depth, and we can see that all AUVs are able to follow their predefined paths at synchronized speeds. Figure 12 depicts the control torques generated by the control laws (26). Although there exist the negative influence caused by unmodelled structure and unknown sea loads, the control torques are bounded and acceptable. Moreover, only two adaptive parameters are required in (26), which alleviates the burdensome computational load. From the local zoom

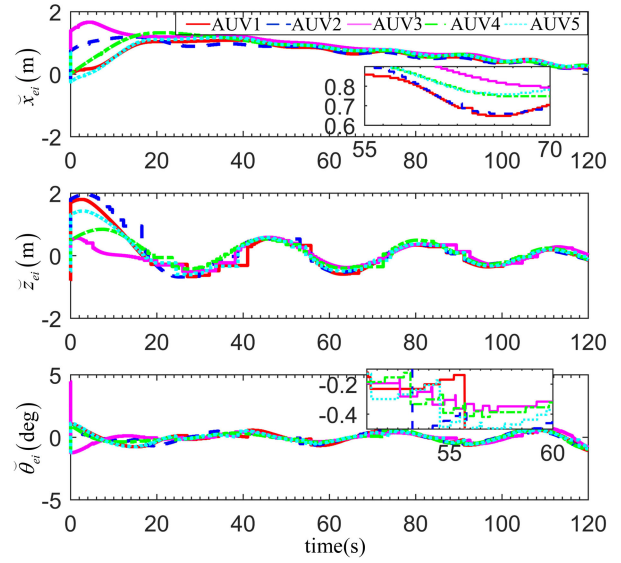


Fig. 10. The curve of tracking errors under varying water depth.

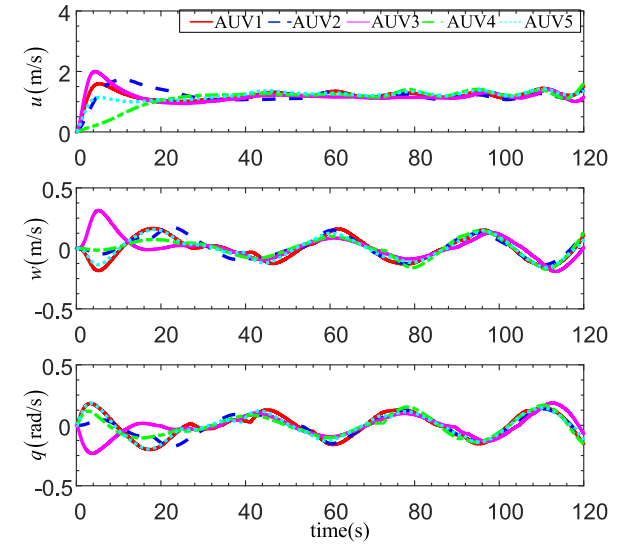


Fig. 11. The curve of velocities under varying water depth.

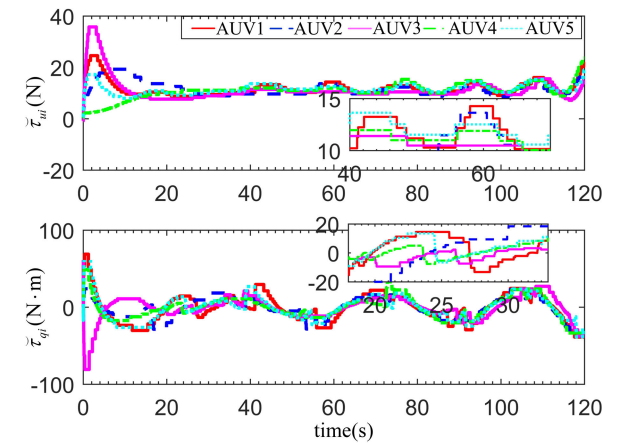


Fig. 12. The curve of control input under varying water depth.

detail, we can found that the curve of control inputs present the stair-stepping form, which can illustrate the effectiveness of the triggering condition in (15). Figure 13 shows the

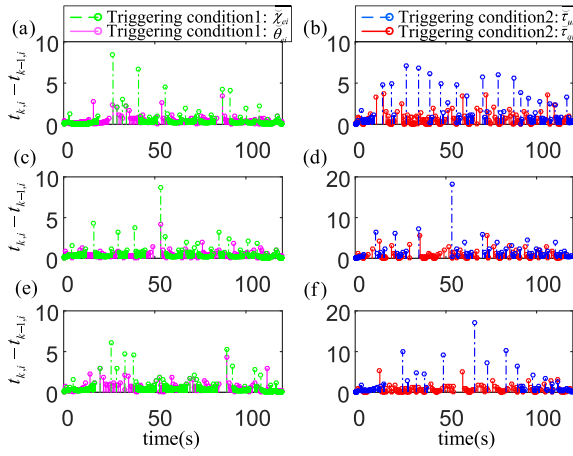


Fig. 13. The interval event time for the proposed DCETM.

triggering instants along the voyage under the proposed DCETM. Without loss of generality, we select the sampling values of the first three AUVs. That is, Fig. 13(a) and (b) represent the triggering instants of AUV1, Fig. 13(c) and (d) denote the triggering instants of AUV2, and Fig. 13(e) and (f) denote the triggering instants of AUV3. The three subgraphs in the first column of Fig. 13 represent the triggering instants under the action of triggering condition for S-C channel (13), while the other three subgraphs denote the triggering instants under the action of triggering condition for C-A channel (15). From the results, we can observe that in the both transient and steady phases, the control signals are aperiodic triggered. During the transient phase, the control signals need to change rapidly to track the reference path, resulting in smaller triggering intervals compared to the steady phase. Above results and analysis are all consistent with Theorem 1.

C. The Comparative Simulation

To further illustrate the effectiveness and the superiority in aspects of the computational burden and the robustness, the comparative simulation is carried out between the proposed DCETM algorithm, the continuous control algorithm and the input-based event-triggered mechanism (INETM) algorithm in [38].

Without loss of generality, one of the underactuated AUVs in Section V-B is selected to express the simulated results more clearly. Figure 14 presents the comparison results of the tracking errors under the different control algorithms. As seen from the Fig.14, it is obvious that the proposed DCETM algorithm and the continuous one have better tracking accuracy than the existing INETM in [38]. Besides, in the locally enlarged view, one can also observe that the curves of the DCETM are with the stair-stepping form, which means that the proposed DCETM scheme is with superiority in the aspect of signal transmission burden. Note that, the continuous scheme seems to have superior tracking performance compared to the proposed DCETM scheme, and this is reasonable since the continuous scheme takes advantage of the real-time location information of the AUV. Referring to Fig.15, it can be shown that the proposed DCETM algorithm demonstrates superior energy-saving performance compared to the contin-

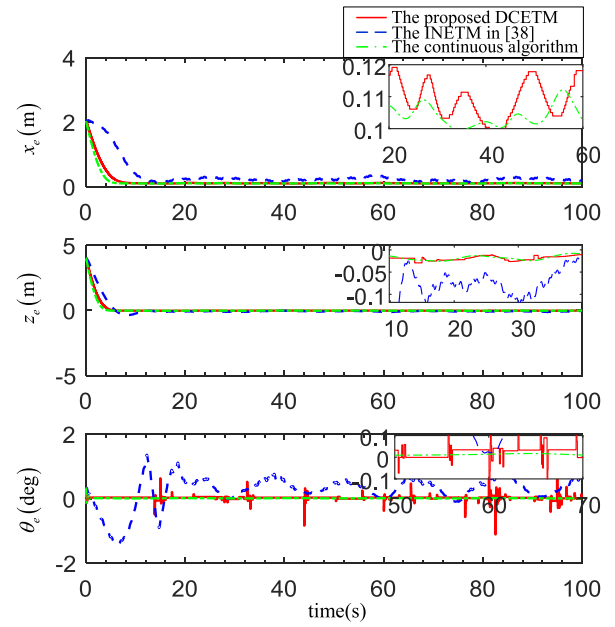


Fig. 14. Comparison of the tracking errors: the proposed DCETM scheme, the continuous scheme and the INETM in [38].

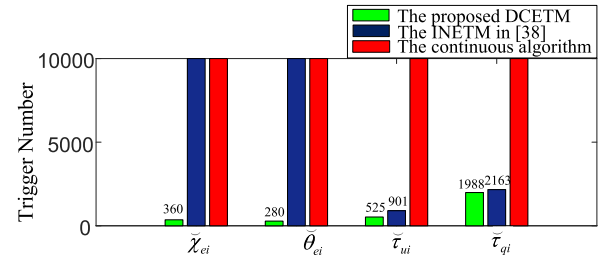


Fig. 15. Comparison of the occupancy frequency of the communication channel: the proposed DCETM scheme, the continuous scheme and the INETM in [38].

uous control algorithm and the INETM algorithm presented in [38]. Despite the INETM algorithm in [38] exhibiting effective energy savings in the C-A channel, with $\tilde{\tau}_{ui}$ and $\tilde{\tau}_{qi}$ triggering 901 and 2163 times respectively, it continues to experience continuous triggering in the S-C channel, with $\tilde{\chi}_{ei}$ and $\tilde{\theta}_{ei}$ triggering 10,000 times respectively. This implies that although the INETM algorithm proposed in [38] can reduce the communication frequency of C-A channel and thus reduce the wear of execution equipment, it ignores the frequent occupation of the S-C channel. Fortunately, under the influence of the DCETM algorithm, $\tilde{\chi}_{ei}$, $\tilde{\theta}_{ei}$, $\tilde{\tau}_{ui}$ and $\tilde{\tau}_{qi}$ trigger 360, 280, 525, and 1988 times respectively, which can reduce the communication frequency in both channels and further conserve the communication channel bandwidth.

For the quantitative purpose, some other important indicators have been added in the comparison simulation to evaluate the corresponding control algorithms. In the Table II, the four performance indexes are introduced to evaluate the corresponding control schemes, i.e., the mean absolute error (MAE), the accumulation of communication data (ACD), the number of adaptive parameter (NAP) and the total event-triggered number (ETN). It is obvious that the proposed DCETM algorithm and the continuous algorithm have the

TABLE II

QUANTITATIVE RESULTS FOR THE PROPOSED CONTINUOUS SCHEME, THE ETC SCHEME AND THE ONE IN [38]

Indexes	Items	The proposed DCETM	The continuous algorithm	The result in [38]
MAE	\tilde{x}_e (m)	0.158	0.139	0.344
	\tilde{z}_e (m)	0.086	0.072	0.184
	$\tilde{\theta}_e$ (deg)	0.044	0.013	0.436
ACD	/	26.7 kb	342.5 kb	235.6 kb
NAP	/	2	2	54
ETN	/	3153	40000	23064

better control accuracy than the INETM algorithm in [38]. Note that, the control accuracy of the continuous algorithm is higher than that of the DCETM algorithm, which is a reasonable phenomenon is caused by the event-triggered mechanism. Furthermore, the proposed DCETM algorithm is superior to the INETM algorithm and the continuous control algorithm in the aspect of complexity and energy saving. As the result, it can be easy to conclude that the proposed DCETM algorithm is with lower communication load and less channel occupancy.

VI. CONCLUSION

This paper investigates the adaptive dual-channel event-triggered control problem for AUVs in the presence of obstacle avoidance, unmolded structures and unknown sea loads. To address obstacle scenarios, the MAPF planning algorithm adjusts the reference path dynamically to accommodate both moving and static obstacles, which can avoid the formation splitting and avoiding collision. In the controller module, the unmoulded structure and unknown sea loads are tackled by fusing of the FS and the one-parameter integrated learning approach. Besides, the DCETM is introduced to reduce the transmission load and actuator execution frequency. Compared with the existing ETC methods, the DCETM ensures both the S-C and C-A channels trigger aperiodically, leading to efficient communication bandwidth usage. Simulation results substantiated the effectiveness and superiority of the proposed control scheme for the formation tracking and obstacle avoidance.

REFERENCES

- [1] T. I. Fossen, *Handbook of Marine Craft Hydrodynamics and Motion Control*. Hoboken, NJ, USA: Wiley, 2011.
- [2] K. D. Do and J. Pan, *Control of Ships and Underwater Vehicles: Design for Underactuated and Nonlinear Marine Systems*. London, U.K.: Springer, 2009.
- [3] Z. Zhou, J. Liu, and J. Yu, "A survey of underwater multi-robot systems," *IEEE/CAA J. Autom. Sinica*, vol. 9, no. 1, pp. 1–18, Jan. 2022.
- [4] J. Wu, C. Song, J. Ma, J. Wu, and G. Han, "Reinforcement learning and particle swarm optimization supporting real-time rescue assignments for multiple autonomous underwater vehicles," *IEEE Trans. Intell. Transp. Syst.*, vol. 23, no. 7, pp. 6807–6820, Jul. 2022.
- [5] J. Yan, X. Zhou, X. Yang, Z. Shang, X. Luo, and X. Guan, "Joint design of channel estimation and flocking control for multi-AUV-based maritime transportation systems," *IEEE Trans. Intell. Transp. Syst.*, vol. 24, no. 12, pp. 14520–14535, Dec. 2023.
- [6] T. Balch and R. C. Arkin, "Behavior-based formation control for multi-robot teams," *IEEE Trans. Robot. Autom.*, vol. 14, no. 6, pp. 926–939, Dec. 1998.
- [7] E. Yang and D. Gu, "Nonlinear formation-keeping and mooring control of multiple autonomous underwater vehicles," *IEEE/ASME Trans. Mechatronics*, vol. 12, no. 2, pp. 164–178, Apr. 2007.
- [8] R. Cui, S. Sam Ge, B. Voon Ee How, and Y. Sang Choo, "Leader-follower formation control of underactuated autonomous underwater vehicles," *Ocean Eng.*, vol. 37, nos. 17–18, pp. 1491–1502, Dec. 2010.
- [9] G. Zong, H. Sun, and S. K. Nguang, "Decentralized adaptive neuro-output feedback saturated control for INS and its application to AUV," *IEEE Trans. Neural Netw. Learn. Syst.*, vol. 32, no. 12, pp. 5492–5501, Dec. 2021.
- [10] S.-M. Wang, M.-C. Fang, and C.-N. Hwang, "Vertical obstacle avoidance and navigation of autonomous underwater vehicles with H_∞ controller and the artificial potential field method," *J. Navigat.*, vol. 72, no. 1, pp. 207–228, Jan. 2019.
- [11] Z. Chu, F. Wang, T. Lei, and C. Luo, "Path planning based on deep reinforcement learning for autonomous underwater vehicles under ocean current disturbance," *IEEE Trans. Intell. Veh.*, vol. 8, no. 1, pp. 108–120, Jan. 2023.
- [12] S. H. Alamdari, G. C. Karras, P. Marantos, and K. J. Kyriakopoulos, "A robust predictive control approach for underwater robotic vehicles," *IEEE Trans. Control Syst. Technol.*, vol. 28, no. 6, pp. 2352–2363, Nov. 2020.
- [13] E. Taheri, M. H. Ferdowsi, and M. Danesh, "Closed-loop randomized kinodynamic path planning for an autonomous underwater vehicle," *Appl. Ocean Res.*, vol. 83, pp. 48–64, Feb. 2019.
- [14] J. Lv, Y. Wang, S. Wang, X. Bai, R. Wang, and M. Tan, "A collision-free planning and control framework for a biomimetic underwater vehicle in dynamic environments," *IEEE/ASME Trans. Mechatronics*, vol. 28, no. 3, pp. 1415–1424, Jun. 2023.
- [15] K. D. Do, "Robust adaptive tracking control of underactuated ODINs under stochastic sea loads," *Robot. Auton. Syst.*, vol. 72, no. 1, pp. 152–163, Oct. 2015.
- [16] J. Li, J. Du, Y. Sun, and F. L. Lewis, "Robust adaptive trajectory tracking control of underactuated autonomous underwater vehicles with prescribed performance," *Int. J. Robust Nonlinear Control*, vol. 29, no. 14, pp. 4629–4643, Sep. 2019.
- [17] I. Eski and S. Yildirim, "Design of neural network control system for controlling trajectory of autonomous underwater vehicles," *Int. J. Adv. Robotic Syst.*, vol. 11, no. 7, Jan. 2014, Art. no. 56740.
- [18] Z. Peng and J. Wang, "Output-feedback path-following control of autonomous underwater vehicles based on an extended state observer and projection neural networks," *IEEE Trans. Syst., Man, Cybern., Syst.*, vol. 48, no. 4, pp. 535–544, Apr. 2018.
- [19] Z. Zhang and Y. Wu, "Adaptive fuzzy tracking control of autonomous underwater vehicles with output constraints," *IEEE Trans. Fuzzy Syst.*, vol. 29, no. 5, pp. 1311–1319, May 2021.
- [20] L. Qiao and W. Zhang, "Trajectory tracking control of AUVs via adaptive fast nonsingular integral terminal sliding mode control," *IEEE Trans. Ind. Informat.*, vol. 16, no. 2, pp. 1248–1258, Feb. 2020.
- [21] H. Wei, C. Shen, and Y. Shi, "Distributed Lyapunov-based model predictive formation tracking control for autonomous underwater vehicles subject to disturbances," *IEEE Trans. Syst., Man, Cybern., Syst.*, vol. 51, no. 8, pp. 5198–5208, Aug. 2021.
- [22] D. Zhao, R. Stobart, and B. Mason, "Real-time energy management of the electric turbocharger based on explicit model predictive control," *IEEE Trans. Ind. Electron.*, vol. 67, no. 4, pp. 3126–3137, Apr. 2020.
- [23] J. Lan, D. Zhao, and D. Tian, "Data-driven robust predictive control for mixed vehicle platoons using noisy measurement," *IEEE Trans. Intell. Transp. Syst.*, vol. 24, no. 6, pp. 6586–6596, Jun. 2021.
- [24] L. Xing, C. Wen, Z. Liu, H. Su, and J. Cai, "Adaptive compensation for actuator failures with event-triggered input," *Automatica*, vol. 85, pp. 129–136, Nov. 2017.
- [25] C.-H. Zhang and G.-H. Yang, "Event-triggered adaptive output feedback control for a class of uncertain nonlinear systems with actuator failures," *IEEE Trans. Cybern.*, vol. 50, no. 1, pp. 201–210, Jan. 2020.
- [26] L. Ma, Y.-L. Wang, and Q.-L. Han, "Event-triggered dynamic positioning for mass-switched unmanned marine vehicles in network environments," *IEEE Trans. Cybern.*, vol. 52, no. 5, pp. 3159–3171, May 2022.
- [27] G. Zhu, Y. Ma, Z. Li, R. Malekian, and M. Sotelo, "Event-triggered adaptive neural fault-tolerant control of underactuated MSVs with input saturation," *IEEE Trans. Intell. Transp. Syst.*, vol. 23, no. 7, pp. 7045–7057, Jul. 2022.
- [28] Y. Deng, Z. Zhang, M. Gong, and T. Ni, "Event-triggered asymptotic tracking control of underactuated ships with prescribed performance," *IEEE Trans. Intell. Transp. Syst.*, vol. 24, no. 1, pp. 645–656, Jan. 2023.

- [29] L. Wen, S. Yu, Y. Zhao, and Y. Yan, "Event-based secure consensus of multiple auvs under dos attacks," *Nonlinear Dyn.*, vol. 107, no. 3, pp. 2407–2419, 2022.
- [30] Y. Shi, W. Xie, M. Xiong, and W. Zhang, "Neural adaptive quantitative prescribed performance sectionalized event-triggered control for autonomous underwater vehicles," *IEEE Trans. Intell. Transp. Syst.*, vol. 24, no. 10, pp. 10857–10868, Oct. 2023.
- [31] K. Chen, G. Luo, H. Zhou, and D. Zhao, "Research on formation control method of heterogeneous AUV group under event-triggered mechanism," *Mathematics*, vol. 10, no. 9, p. 1373, Apr. 2022.
- [32] Y. Deng, T. Liu, and D. Zhao, "Event-triggered output-feedback adaptive tracking control of autonomous underwater vehicles using reinforcement learning," *Appl. Ocean Res.*, vol. 113, Aug. 2021, Art. no. 102676.
- [33] C. L. P. Chen, G.-X. Wen, Y.-J. Liu, and Z. Liu, "Observer-based adaptive backstepping consensus tracking control for high-order nonlinear semi-strict-feedback multiagent systems," *IEEE Trans. Cybern.*, vol. 46, no. 7, pp. 1591–1601, Jul. 2016.
- [34] Y. Li, S. Tong, and T. Li, "Adaptive fuzzy output feedback dynamic surface control of interconnected nonlinear pure-feedback systems," *IEEE Trans. Cybern.*, vol. 45, no. 1, pp. 138–149, Jan. 2015.
- [35] B. K. Sahu and B. Subudhi, "Flocking control of multiple AUVs based on fuzzy potential functions," *IEEE Trans. Fuzzy Syst.*, vol. 26, no. 5, pp. 2539–2551, Oct. 2018.
- [36] S. S. Ge and Y. J. Cui, "New potential functions for mobile robot path planning," *IEEE Trans. Robot. Autom.*, vol. 16, no. 5, pp. 615–620, Oct. 2000.
- [37] W. Dong and Y. Guo, "Global time-varying stabilization of underactuated surface vessel," *IEEE Trans. Autom. Control*, vol. 50, no. 6, pp. 859–864, Jun. 2005.
- [38] G. Zhang, S. Chu, X. Jin, and W. Zhang, "Composite neural learning fault-tolerant control for underactuated vehicles with event-triggered input," *IEEE Trans. Cybern.*, vol. 51, no. 5, pp. 2327–2338, May 2021.

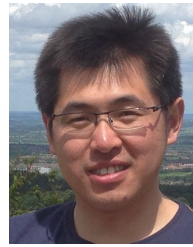


Shang Liu received the B.S. degree from Jimei University, Xiamen, China, in 2020, and the M.S. degree from Dalian Maritime University, Dalian, China, in 2023. He is currently pursuing the Ph.D. degree with Northeastern University, Shenyang, China. He is also a Visiting Research Assistant with Guangdong Key Laboratory of Intelligent Transportation System, School of Intelligent Systems Engineering, Sun Yat-sen University, Guangzhou, China. His research interests include adaptive control, event-triggered control, nonlinear control, and their applications on intelligent vehicles.



Ronghui Zhang received the B.Sc. (Eng.) degree from the Department of Automation Science and Electrical Engineering, Hebei University, Baoding, China, in 2003, the M.S. degree in vehicle application engineering from Jilin University, Changchun, China, in 2006, and the Ph.D. (Eng.) degree in mechanical and electrical engineering from Changchun Institute of Optics, Fine Mechanics and Physics, The Chinese Academy of Sciences, Changchun, in 2009. After finishing the Post-Doctoral Research Work at INRIA, Paris,

France, in February 2011, he is currently an Associate Professor with Guangdong Key Laboratory of Intelligent Transportation System, School of intelligent systems engineering, Sun Yat-sen University, Guangzhou, Guangdong, China. His current research interests include computer vision, intelligent control, and ITS.



Dezong Zhao (Senior Member, IEEE) received the B.Eng. and M.S. degrees in control engineering from Shandong University in 2003 and 2006, respectively, and the Ph.D. degree in control engineering from Tsinghua University in 2010. Since 2023, he has been a Reader in autonomous systems with the University of Glasgow. His research interests include connected and autonomous vehicles, robotics, machine learning, and control engineering. He has been an EPSRC Innovation Fellow since 2018 and a Royal Society-Newton Advanced Fellow since 2020.



Houbing Song (Fellow, IEEE) received the Ph.D. degree in electrical engineering from the University of Virginia, Charlottesville, VA, USA, in August 2012. He is currently a Tenured Associate Professor, the Director of the NSF Center for Aviation Big Data Analytics (Planning), the Associate Director for Leadership of the DOT Transportation Cybersecurity Center for Advanced Research and Education (Tier 1 Center), and the Director of the Security and Optimization for Networked Globe Laboratory (SONG Lab, www.SONGLab.us), University of Maryland,

Baltimore County (UMBC), Baltimore, MD, USA. Prior to joining UMBC, he was a tenured Associate Professor of Electrical Engineering and Computer Science at Embry-Riddle Aeronautical University, Daytona Beach, FL, USA. He is an editor of eight books, the author of more than 100 articles, and an inventor of two patents. His research has been sponsored by federal agencies (including National Science Foundation, National Aeronautics and Space Administration, U.S. Department of Transportation, and Federal Aviation Administration), and industry. His research has been featured by popular news media outlets, including IEEE GlobalSpec's Engineering360, Association for Uncrewed Vehicle Systems International (AUVERSI), Security Magazine, CXOTech Magazine, Fox News, U.S. News and World Report, The Washington Times, and New Atlas. His research interests include cyber-physical systems/Internet of Things, cybersecurity and privacy, and AI/machine learning/big data analytics. He has been serving as an Associate Editor for IEEE TRANSACTIONS ON ARTIFICIAL INTELLIGENCE since 2023, IEEE INTERNET OF THINGS JOURNAL since 2020, IEEE TRANSACTIONS ON INTELLIGENT TRANSPORTATION SYSTEMS since 2021, and IEEE JOURNAL ON MINIATURIZATION FOR AIR AND SPACE SYSTEMS since 2020. He was an Associate Technical Editor for *IEEE Communications Magazine* from 2017 to 2020. He is an IEEE Fellow (for contributions to big data analytics and integration of AI with Internet of Things) and an ACM Distinguished Member (for outstanding scientific contributions to computing). He has been an ACM Distinguished Speaker since 2020 and an IEEE Vehicular Technology Society (VTS) Distinguished Lecturer since 2023. He has been a Highly Cited Researcher identified by Clarivate™ in 2021 and 2022 and a Top 1000 Computer Scientist identified by Research.com. He received Research.com Rising Star of Science Award in 2022 (World Ranking: 82; U.S. Ranking: 16). He was a recipient of more than ten best paper awards from major international conferences, including IEEE CPSCOM-2019, IEEE ICII 2019, IEEE/AIAA ICNS 2019, IEEE CBDCOM 2020, WASA 2020, AIAA IEEE DASC 2021, IEEE GLOBECOM 2021, and IEEE INFOCOM 2022.